POLITECNICO DI TORINO
Repository ISTITUZIONALE

Comparison of hydrogen-fueled powertrains for urban bus applications — design, modeling, and energy management

Original
Comparison of hydrogen-fueled powertrains for urban bus applications — design, modeling, and energy management / Pulvirenti, L., Rolando, L., Vinogradov, A., Peiretti Paradisi, B.. - In: INTERNATIONAL JOURNAL OF HYDROGEN ENERGY. - ISSN 0360-3199. - 110:(2024), pp. 560-574. [10.1016/j.ijhydene.2025.02.004]

Availability:
This version is available at: 11583/2997769 since: 2025-02-28T08:41:46Z

Publisher:
Elsevier

Published
DOI:10.1016/j.ijhydene.2025.02.004

Terms of use:

This article is made available under terms and conditions as specified in the corresponding bibliographic description in the repository

Publisher copyright

(Article begins on next page)

28 November 2026

International Journal of Hydrogen Energy 110 (2024) 560–574

Contents lists available at ScienceDirect

International Journal of Hydrogen Energy

journal homepage: www.elsevier.com/locate/he

Comparison of hydrogen-fueled powertrains for urban bus applications — design, modeling, and energy management

Luca Pulvirenti, Luciano Rolando *, Afanasie Vinogradov, Benedetta Peiretti Paradisi

Politecnico di Torino, Corso Duca degli Abruzzi, 24, Torino, 10129, Italy

ARTICLE INFO

Keywords:
Hydrogen powertrain
HEV
Urban bus
Fuel cell
Energy management strategy
Equivalent Consumption Minimization Strategy

ABSTRACT

Nowadays, there is a growing consensus that hydrogen can play a key role in decarbonizing Heavy-Duty Vehicle (HDV) fleets as it can be produced from renewable energy sources and supply both Internal Combustion Engines (ICEs) and Fuel Cells (FCs). This research paper proposes a fair and comprehensive comparison between two different hybrid H_2-fueled powertrains for urban bus applications. The two case studies are a H_2-Hybrid Electric Vehicle (HEV) featuring an ICE and a Fuel Cell Electric Vehicle (FCEV). We thoroughly modeled the hybrid H_2-fueled powertrains, paying particular attention to the development of their energy management strategies. We adopted a standard Equivalent Consumption Minimization Strategy (ECMS) for the H_2-HEV. For the FCEV, where the FC aging represents a limit to reach competitiveness with H_2-ICE, we developed a modified version ($ECMS_{w/deg}$) designed to both limit FC degradation and minimize fuel consumption. Finally, we benchmarked the energy consumption of the hybrid H_2-fueled powertrains, on a Tank-To-Wheel (TTW) basis, against a conventional ICE vehicle, a diesel HEV, and a Battery Electric Vehicle (BEV). This work demonstrates that hybrid H_2-fueled powertrains can represent valid pathways to decarbonize urban bus fleets, allowing to reduce the energy consumption of a diesel ICE bus by an average of 29% (H_2-HEV), and 42% (FCEV).

1. Introduction

In response to the looming concerns regarding global warming, regulators are imposing stringent limitations to curb the increasing trend of Greenhouse Gas (GHG) emissions. Within the EU, the transportation sector accounts for roughly 35% of the total worldwide energy consumption [1]. Specifically, road transport stands out as one of the most important contributors, constituting 77% of the overall GHG emissions coming from the transportation sector [2], with Heavy Duty Vehicles (HDVs) being responsible for more than a quarter of these emissions [3]. In this framework, the European Commission has set the ambitious target of achieving net zero GHG emissions by 2050 [4]. Moreover, in 2023 it proposed a revision of the current regulation for HDVs by introducing stringent CO_2 emission targets from 2030 onward and extending it to cover smaller trucks, city and long-distance buses, and trailers. The proposal establishes a 90% decrease in CO_2 emissions per km from new HDVs by 2040 (compared to a mid-2019 to mid-2020 baseline) with intermediate targets for 2030 (45%) and 2035 (65%) [5].

A shift toward more sustainable vehicle propulsion systems is required to achieve compliance with current legislation targets and future proposals, and powertrain electrification represents one of the most promising solutions to decarbonize the current fleets of Light-Duty Vehicles (LDVs) [6]. However, despite their impressive recent developments, Battery Electric Vehicles (BEVs) may encounter more challenges when deployed for other applications, such as trucks, buses, and commercial vehicles, due to their high capital costs, low battery-energy densities (hence limited ranges), payload reduction, long recharging time, and lack of recharging infrastructure [7,8].

Among the available alternatives, hydrogen offers a versatile, potentially clean, and flexible energy vector that can play a key role in decarbonizing the HDV segment [9,10], and particularly the city bus networks [11,12]. Hydrogen has long attracted special attention since it can obtain zero tailpipe pollutants and GHG emissions, achieve high energy efficiency, and rely on renewable energy sources [13]. However, a mass-scale adoption of hydrogen-based technologies requires an adequate infrastructure to supply continuous hydrogen production at a reasonable cost and with minimum carbon footprint [14,15], and still needs to overcome challenging barriers: although prices of H_2-based technologies are decreasing over time, they are still significantly higher than those of conventional technologies [16].

H_2-fueled powertrains can utilize two main energy conversion technologies: Fuel Cell (FC) and Internal Combustion Engine (ICE). Fuel Cell Electric Vehicles (FCEVs), currently the most widely commercialized hydrogen-based solution, are particularly promising due to their

* Corresponding author.
E-mail address: luciano.rolando@polito.it (L. Rolando).

https://doi.org/10.1016/j.ijhydene.2025.02.004
Received 24 October 2024; Received in revised form 23 December 2024; Accepted 1 February 2025
Available online 20 February 2025
0360-3199/© 2025 The Authors. Published by Elsevier Ltd on behalf of Hydrogen Energy Publications LLC. This is an open access article under the CC BY-NC-ND license (http://creativecommons.org/licenses/by-nc-nd/4.0/).

high overall energy efficiency, rapid refueling capability, extended driving ranges, and absence of tailpipe emissions [17]. In particular, fast refueling time in combination with long driving range can significantly decrease the need for a widespread refueling infrastructure, which is very relevant in the early stage of their deployment [16]. However, their limited production volumes, as well as the need for precious materials for the FC components, may still result in quite high capital investment, especially in a short-time scenario. Moreover, if compared to BEV technologies, FCEVs are characterized by lower overall efficiency.

On the other hand, H_2-fueled ICE emerges as a Total Cost of Ownership (TCO)-competitive technology thanks to the limited number of hardware changes required from conventional ICEs and to the availability of well-established production processes [18,19]. Moreover, compared to FC systems, H_2-ICEs can tolerate a higher level of impurities in the fuel and can switch between different fuels, thus also allowing for decarbonizing vehicle segments where hydrogen supply infrastructure has not yet achieved full coverage [20]. On the contrary, the main drawback of an H_2-fueled ICE is the generation of pollutant emissions, such as Nitrogen Oxides (NO_x), which may require tailored after-treatment devices [21]. For what concerns the energy conversion efficiency, the H_2-ICE cannot compete with the FC at low loads. However, it can achieve similar efficiency levels at high loads, making both these technologies suitable for HDV applications [22].

For some specific applications, such as urban buses, the hybridization of H_2-fueled powertrains can further reduce their energy consumption and therefore GHG emissions [23]. More specifically, a series-hybrid design, in which the FC system or the ICE is considered as an Auxiliary Power Unit (APU), and thus decoupled from the wheels, is particularly advantageous since urban transit applications comprise continuous start-and-stop and driving patterns at low average speeds. For an FCEV, allowing the FC to operate independently from the power demand is not only beneficial in terms of fuel economy [24] but also in terms of degradation: the frequent starts-and-stops, as well as load fluctuations, lead to oxygen starvation, membrane dehydration, and other phenomena that accelerate the FC aging [25,26].

Nevertheless, due to the increased complexity of Hybrid Electric Vehicles (HEVs), the benefits provided by hybridization may be jeopardized if the cooperation between the power actuators is not optimized. Therefore, an additional level, namely the Energy Management System (EMS), must be added to the vehicle control hierarchy to optimize the power split between the power actuators [27]. The EMS of an FCEV should also consider FC aging to guarantee long-lasting operation and thus reach competitiveness in terms of TCO with Internal Combustion Engine Vehicles (ICEVs) and BEVs. This rings particularly true for HDVs where the useful life of the powertrain components and the TCO are among the primary selling points. Optimizing the physical operating conditions of the FC such as temperature optimization [28] and effective water management [29] are crucial in extending its operational life. However, how power is provided by the FC plays an equally significant role in the durability and overall performance. While the EMS may not directly and explicitly measure and evaluate the FC deterioration, it can be aware of the degradation rates of the FC based on the operating conditions. This enables the EMS to optimize the power split, ensuring fuel economy and longevity.

Nevertheless, considering the FC degradation rate in the EMS requires modeling complex mechanisms highly dependent on its design and materials. Two approaches can be adopted: the first one, based on physical models [30], is typically used in the development and assessment phases. This approach calculates FC degradation from the first principle methods. It is computationally demanding and does not directly relate degradation phenomena to operating conditions, thus it is not feasible for energy management usage and online controls. The second approach, based on empirical models [31], correlates performance losses to operating conditions through observations of FC usage. Although less accurate, this approach is more suitable for online control. A significant contribution to the empirical modeling was given by Pei et al. in [32], which proposed an arithmetic equation of FC lifetime correlated to its operating conditions such as load, start and stop, and load variation under real driving conditions of an urban bus.

Surveying the literature, the first health-conscious EMSs just protected the FC by limiting its operation. For example, in [33], a DC-DC converter was used in an urban bus to gradually adjust the output power of the FC stacks and thus extend its lifetime. Other works, as in [34], tried to minimize operation under conditions leading to high degradation rates, such as high loads or the number of load changes. However, many state-of-the-art health-conscious EMSs available in the literature use a formulation derived with some adaptations from [32], to quantify the dependency of the degradation rate on the driving conditions (acceleration, idling, etc.). For example, degradation formulations derived from [32] were integrated by Tang et al. [35] in the reward function of a deep reinforcement learning controller. Similar formulations were used also by Luca et al. [36] for a fuzzy logic aimed at prolonging the FC lifetime, or by Wang et al. [37] that added more details in the modeling of the low voltage degradation region in its EMS. In this framework, Desantes et al. [38] added a major contribution to the empirical models by including the dependency of FC degradation on some fundamental physical variables such as relative humidity and temperature. Moreover, they proposed an equation to evaluate the impact of load level on degradation spanning the entire load request range and the possibility of evaluating the degradation to a continuous load change variation. This formulation was then used in [39] to develop a predictive Equivalent Consumption Minimization Strategy (ECMS) that used speed prediction and various dynamic constraints to mitigate FC degradation.

1.1. Knowledge gaps

Throughout the reviewed literature, the following observations can be made:

- Despite the increasing interest in H_2-fueled powertrains, research on FCEVs and H_2-ICEVs is typically conducted independently. Numerous studies focus on the performance of H_2-engines [40,41] or FC stacks and their EMSs [24,33], in some cases also taking into account FC degradation [35,42]. However, all these works leave a clear gap in the scientific literature for direct comparisons between these two powertrain technologies. A comparative analysis of H_2-fueled powertrains is of great importance for determining the most suitable H_2-fueled power generation system. Quite recently some papers have tried to fill this gap by comparing these two powertrain technologies [43–47]. More specifically, Singh et al. [43] performed an extensive literature review on the utilization of H_2 in ICEVs and FCEVs. In [44], an FC and a H_2-ICE were carefully compared in techno-enviro-economic terms. Careful attention was paid to several different aspects, however, they did not consider any specific applications, e.g., vehicles. Durkin et al. [45] designed and modeled an FC versus an H_2-ICE for passenger car applications. However, they did not consider any aging of the FC, and adopted efficiency maps of conventional engines for the H_2-ICE. Depcik et al. [46] assessed the possibility of adopting H_2-fueled ICE and FC for a small unmanned aerial vehicle. Finally, Sari et al. [47] compared H_2-fueled ICE and FC for long haul applications. For bus applications FCEV are often compared to BEVs or ICEs [10,24,48,49] but hydrogen fuel potential in different technologies such as ICE and FC is not comprehensively investigated. In the literature, to the best of our knowledge, a direct comparison between H_2-ICE and FC for bus applications is still missing.
- Emission reduction as well as techno-economical analyses of fleets of H_2-fueled powertrains are abundant in the literature [11,50], but they lack essential questions about their EMSs, and often rely

on simplistic tabular data for their analyses. In these works, hypotheses are often done about average constant operations of the H_2-fueled powertrains, without taking into account comprehensive aspects for each powertrain, such as increased fuel consumption and reduced lifetime of an FC due to its degradation [16,24].

- Focusing on FCEV, many health-conscious EMSs available in the literature make the simplistic assumption that degradation occurs only at low and high loads, but not at moderate loads [35–37]. Moreover, some of them only consider degradation when discrete load changes exceed a certain threshold of variation [36,37]. However, these hypotheses may lead to misleading insights on FC degradation. Moreover, many studies provide simplified durability indicators for showing lifetime improvements, such as the time spent under high load or the number of cycle variations, without addressing the impact of degradation on the overall lifespan of the powertrain [34–36]. Finally, most reviewed works do not consider the impact of FC degradation on the increased power demand requested by the Balance of Plant (BoP) and do not provide information on how degradation affects fuel consumption over the powertrain's lifetime.

1.2. Contribution and objectives

In this paper we address the above-mentioned gaps in the literature by proposing a fair and comprehensive comparison between two different hybrid H_2-fueled powertrains, namely a H_2-ICEV and an FCEV, for urban bus applications. The analysis is carried out on the virtual test rig of a 12 m urban bus through numerical simulation. The design of both powertrain configurations, as well as their modeling, is performed leveraging prior works of the Authors [51–53]. All powertrain components are carefully modeled and validated against experimental data or through detailed 1D–3D CFD simulations. In addition, we conducted a thorough investigation of the literature to generate realistic hypotheses.

The major contributions of the paper can be summarized as follows:

- We analyzed the H_2 consumption of a 12 m urban bus featuring a H_2-ICE and a FC on three different driving cycles. Thorough modeling of all the components allowed us to obtain realistic fuel consumption estimations. To the best of our knowledge, this study is the first to provide such a detailed comparison between H_2-fueled powertrains for urban bus applications.
- Focusing on the FCEV, we calibrated a detailed electrochemical model of the FC stack for a reliable prediction of the system performance. Moreover, a FC degradation modeling is crucial for a realistic estimation of its life expectancy. Therefore, we used an empirical approach derived from [38] for capturing FC stack degradation by considering the most relevant degradation phenomena. Moreover, to correctly estimate FC consumption over its lifetime, we included the negative effect of stack degradation on the BoP. This approach addresses a rarely explored aspect in the literature and it is a crucial input for Life-Cycle Assessments (LCAs) that often rely on FC consumption at the beginning of its operational life.
- We devoted particular attention to the development of energy management strategies tailored for hybrid H_2-fueled powertrains. We proposed an ECMS [54] thanks to both its suboptimal performance and ease of implementation. The EMS of an FCEV should also consider FC aging to guarantee long-lasting operation and thus reach competitiveness with H_2-ICE. For this reason, we developed a modified version of the ECMS, called $ECMS_{w/deg}$, aimed at minimizing fuel consumption while limiting degradation.
- Finally, we used the optimized energy management strategies to assess the viability of the H_2-fueled powertrains from a broader perspective. The investigated H_2-fueled powertrains are compared, with a Tank-To-Wheel (TTW) perspective, against other technologies available in the market: a conventional ICEV, a diesel HEV, and a BEV.

Table 1
Vehicle main specifications.

Length	[m]	12
Curb Weight	[ton]	12
Road Load @ 50 km/h	[kW]	16
Frontal Area	[m^2]	7.6
Aerodynamic Drag	[-]	0.56
Rolling Resistance	[-]	0.006
Max Passengers Capacity	[-]	90

The rest of the paper is organized as follows: Section 2 presents the case study, the different powertrain architectures, and the mission profiles used in the analysis. Section 3 presents the development of the virtual test rig of the vehicle. Section 4 formalizes the developed strategies for the energy management of the two H_2-fueled powertrains. Section 5 shows the performance of the developed control strategies on the adopted driving cycles, paying close attention to the $ECMS_{w/deg}$ in terms of fuel economy and FC life extension. Section 5 also assesses the overall TTW impact of the hybrid H_2-fueled powertrains by benchmarking them against the other configurations. Finally, Section 6 presents the main conclusions and further developments of the research activity.

2. Case study

This Section describes in detail the main features of the simulated 12 m urban bus. The vehicle specifications are summarized in Section 2.1, then the powertrain components are analyzed in 2.2, and, finally, the considered driving cycles are described in Section 2.3.

2.1. Vehicle specifications

For the present work, a standard bus, i.e., a 12 m bus representing 68% of the worldwide urban bus fleets [55], was chosen, and its main specifications are reported in Table 1.

2.2. Powertrain configurations

Since this work aims to provide a comprehensive comparison between H_2-fueled powertrains, it will be mainly focused on these two configurations. However, this Section will provide additional specifications of the other powertrains considered as a benchmark.

In particular, the five different powertrain configurations listed in Table 2 were considered: #1 ICEV; #2 diesel-HEV; #3 H_2-fueled HEV; #4 FCEV; #5 BEV. They all meet the power requirements of the driving scenarios considered in this work and their main specifications are summarized in Table 3. The Conf.#1 is a conventional powertrain equipped with a large displacement diesel engine: it will be used as the benchmark of the TTW analysis as almost 50% of the worldwide urban buses are still propelled by a diesel engine [55]. Moving to the hybrid configurations (Conf.#2, #3, and #4), which are the main focus of this work and are schematically sketched in Fig. 1, they all feature a series architecture where the main power actuator is a 200 kW Permanent Magnet (PM) Electric Machine (EM) powered by a 20 kWh Li–Ion battery. Thanks to its excellent thermal stability, long cycle life, enhanced safety and tolerance, and good power density, Lithium Iron Phosphate (LFP) chemistry was chosen for this application [56,57]. The cell specifications were acquired from [58], while the cell Open Circuit Voltage (OCV) and internal resistance were obtained from [59,60], respectively.

For what concerns the APU, Conf.#2 features a downsized version of the reference diesel engine with a maximum power of about 100 kW. The power unit of the Conf.#3 was obtained by converting the downsized diesel engine to operate with H_2 fuel. The H_2 engine was designed to provide the same rated power while minimizing conversion cost and complexity [51,52]. Both these hybrid configurations feature

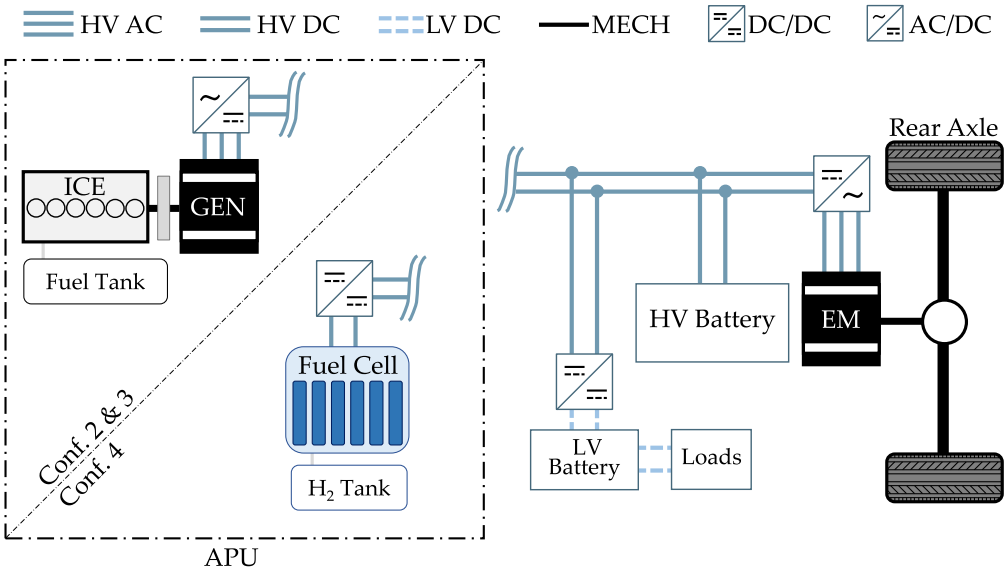


Fig. 1. Schematic layout of the hybrid series configurations. The APU features an ICE for Conf.#2 and #3, and a FC for Conf.#4.

Table 2
Powertrain configurations and their differences in terms of architecture, APU type, and energy carrier.

	Configuration	Architecture	APU	Energy carrier
#1	ICEV	Pure ICE	–	Diesel
#2	HEV	Hybrid Series	ICE	Diesel
#3	H_2-HEV		ICE	H_2
#4	FCEV		Fuel Cell	H_2
#5	BEV	Pure Electric	–	Electricity

Table 3
Main specifications of the analyzed powertrain configurations.

	Configuration	#1	#2	#3
ICE	Fuel [-]	Diesel	Diesel	Hydrogen
	Displacement [cm^3]	Large	Medium	Medium
	Max Power [kW]	250	100	100
	Source [-]	[52]	[52]	[52]
	Configuration	#4		
Fuel cell	Fuel [-]	Hydrogen		
	Net Power [kW]	100		
	Number of Cells [-]	270		
	Source [-]	[53]		
	Configuration	#2#3	#2#3#4#5	
EM	Label [-]	GEN	EM	
	Technology [-]	PMSM	PMSM	
	Max Power [kW]	90	200	
	Max Torque [Nm]	440	1500	
	Source [-]	[61]	[62]	
	Configuration	#2#3#4	#5	
HV battery	Technology [-]	LFP	NCM	
	Capacity [kWh]	20	336	
	Arrangement [-]	120s20p	108s9p	
	Source [-]	[58]	[63]	

an additional 90 kW EM (labeled as GEN in Fig. 1) and an AC/DC converter to feed electric energy to the net. The GEN was chosen to match the ICE rated power and its main characteristics were obtained from [61]. Finally, Conf.#4 was obtained by substituting the APU with an FC system: a real FC system was rescaled to obtain the same power level of Conf.#2 and #3. As shown in Fig. 1, a DC/DC converter is needed to couple the FC with the high-voltage board net of the electrified powertrain. The energy consumption of the FC ancillaries (such as the air compressor and the humidifier) was also considered for the BoP.

Finally, given the recent popularity gained by BEVs in the global market (they constitute more than 6% of the worldwide urban buses [55]), a fully electric powertrain was also included in this study. The BEV features the same power actuator of the hybrid powertrains, but not the same battery chemistry as LFP technology is affected by a limited energy density [56]. A higher energy-density chemistry, namely the Nickel–Cobalt–Manganese (NCM) technology, was adopted to fulfill the range requirements of the BEV. The cell main specifications along with the OCV and internal resistance values were obtained from [63], and the battery capacity was chosen by taking a 12 m e-bus circulating in the city of Turin as a reference [64]. The selected 336 kWh battery capacity allows the bus to achieve a range of about 235 km on the Braunschweig driving cycle (see Section 2.3). It is worth mentioning that the battery weight cannot be neglected in a BEV as it may drastically increase the curb weight of the vehicle, particularly for a bus. In this work, an overall battery weight of about 2500 kg was estimated based on data reported in the literature [65].

2.3. Driving cycles

Realistic speed profiles are essential to obtain realistic results in terms of energy consumption. The comparison of the different propulsive systems is carried out using three different driving cycles, representative of typical urban bus operations. They are depicted in Fig. 2, while their main characteristics are listed in Table 4.

The Braunschweig driving cycle, which has been employed in various research projects or equipment certification programs [66], features a transient driving schedule with frequent stops. The Gillingham cycle was obtained from real-world GPS acquisitions, and, as evident from Fig. 2 and Table 4, it features elevation changes and more challenging driving conditions. Lastly, the Millbrook London Transport Bus (MLTB) Test cycle was developed in 1996 by UK transport authorities to verify the compliance of new vehicles with emissions and fuel economy standards [67]. It features a lower average speed, thus covering a smaller distance in a longer duration, if compared to the Braunschweig. From Table 4 it should be noted that all three driving cycles feature a high share of stop phases (between 22% and 27%) as urban bus applications comprise several start-and-stop driving patterns.

Table 4
Summary of the characteristics of the adopted driving cycles.

		Braunschweig	Gillingham	MLTB
Distance	[km]	10.9	16.6	9.0
Duration	[s]	1740	2875	2281
Avg. Speed	[km/h]	23	21	14
Max Speed	[km/h]	58	60	49
Avg. Acc.	[m/s^2]	0.2	0.2	0.2
Max Acc.	[m/s^2]	2.4	2.3	1.5
Stop Phases	[%]	22	22	27
Const Speed	[%]	16	12	6
Energy Demand	[kWh/100 km]	90	105	94

3. Virtual test rig

The virtual test rig of the bus was developed in the commercial software GT-SUITE®, while Simulink® was employed for developing the control strategies leveraging its superior flexibility for this task. The model relies on a quasi-static approach: a virtual vehicle driver – i.e., a Proportional–Integral–Derivative (PID) controller – generates a power demand profile depending on the difference between actual and target vehicle speed. To ensure that the powertrain provides the power demand required to meet the target speed, the vehicle's longitudinal dynamics [68] were modeled, including aerodynamic drag, rolling resistance, inertia force, and road grade. The ICE and EM models rely on performance maps, that were experimentally measured under steady-state conditions, except from the H_2-ICE ones which were computed from 1D–3D CFD simulations [51]. The battery dynamics were modeled using a Thevenin equivalent circuit, while an electrochemical model was developed for the FC system [69].

For what concerns the Regenerative Braking System (RBS), a serial strategy was implemented as it guarantees better driving comfort and a higher ratio of regeneration if compared with a parallel strategy [70]. A serial strategy guarantees that, under light braking operations, the braking force is directed toward the rear wheels which use the RBS to provide sufficient braking force, while, for higher braking power demands, the force is split between the front and rear axles: this ensures more vehicle stability but, at the same time, drastically reduces the share of recoverable energy.

Since the aim of this work is to explore the capabilities of H_2-fueled powertrains for urban buses application, the following Sections will be devoted to the modeling of the H_2-fueled powertrains, i.e., Conf.#3 and #4, and to the development of their energy management strategies.

3.1. Conf.#3: H2-ICE model

The H_2-ICE was modeled through performance maps obtained from a combined 1D–3D CFD workflow. Initially, 3D-CFD simulations, featuring a detailed chemistry scheme for both hydrogen combustion and NO_x emissions, provided combustion insights and performance. The results were used to calibrate a predictive 1D-CFD combustion model as described in [52]. Once calibrated, the 1D-CFD model was used as a virtual test rig to optimize the main operating parameters (e.g., air/fuel ratio, boost level, and spark timing) in order to maximize the engine thermal efficiency, achieving a peak of about 41%, while ensuring, at the same time, compliance with the EU6 NO_x emissions limit for HDVs applications.

3.2. Conf.#4: Fuel cell model

The FC stack model integrates the fluid dynamics domain with the electrochemistry one. It exploits the well-established 1D simulation approach for solving fluid dynamics of air and hydrogen paths. Simultaneously, the electrochemical model is used for evaluating stack voltage for given current and operating conditions:

$$V_{\text{cell}} = V_{\text{ocv}} - V_{\text{act}} - V_{\text{ohm}} - V_{\text{conc}} \tag{1}$$

where:

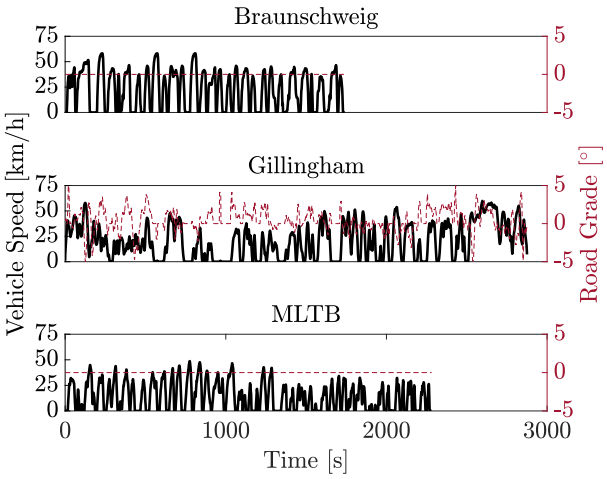


Fig. 2. Vehicle speed (black line) and road grade (red dotted line) plotted as a function of time for the three driving cycles used in the simulations.

- V_{ocv} is the OCV at null current;
- V_{act} represents the activation losses associated with electrochemical reaction, and can be described by the Tafel equation:

$$V_{\text{act}} = \begin{cases} \frac{RT}{2F}\left(\frac{i}{i_0}\right) & \text{if } i \le \frac{i_0}{1-\alpha}, \\ \frac{RT}{2\alpha F}\ln\left(\frac{i}{i_0}\right) & \text{if } i > \frac{i_0}{1-\alpha}, \end{cases} \tag{2}$$

  where i is the current density and i_0 is the exchange current density, depending on the reference exchange current and on the temperature and partial pressure of the reactants at the catalyst layer [71];
- V_{ohm} represents the losses associated with the protonic conductivity, and can be expressed by the Ohm law:

$$V_{ohm} = R_i i \tag{3}$$

  where R_i is the internal resistance and highly depends on membrane humidification. The membrane resistance is modeled using the Springer–Zawodzinski formulation [72];
- V_{conc} represents the concentration losses that occur when the requested current exceeds the diffusion rate of reactants. This term is modeled through the limiting current i_L:

$$V_{conc} = \frac{RT}{nF}\ln\left(\frac{i_L}{i_L - i}\right) \tag{4}$$

The FC model was calibrated by adjusting key parameters, such as the reference exchange current density ($i_{0,ref}$) and the parameters associated with the membrane conductivity affecting the internal resistance R_i. Fig. 3 shows the simulated polarization curve of the FC model (blue solid line) against experimental data (black dashed line) of a single cell of the FC stack. The more than satisfactory agreement between the simulation results and the experimental measurements proves the robustness of the developed model.

Once the stack model was calibrated, it was integrated into a system with all the ancillaries needed to guarantee the correct operation of the stack as depicted in Fig. 4(a). The anode receives the proper amount of air from the compressor, compensating for any pressure losses. The humidifier controls the water content to curb membrane degradation. The dry hydrogen coming from the tank storage is mixed, in the recirculation pump, with the humid hydrogen exiting from the anode, and is then fed to the inlet. All the flow components, such as the humidifier, were modeled through a 1D-CFD approach, while only the compressor and the H_2 recirculation pump were modeled through 0D performance maps. Finally, a 1% penalty was added to the system efficiency to account for hydrogen purging losses.

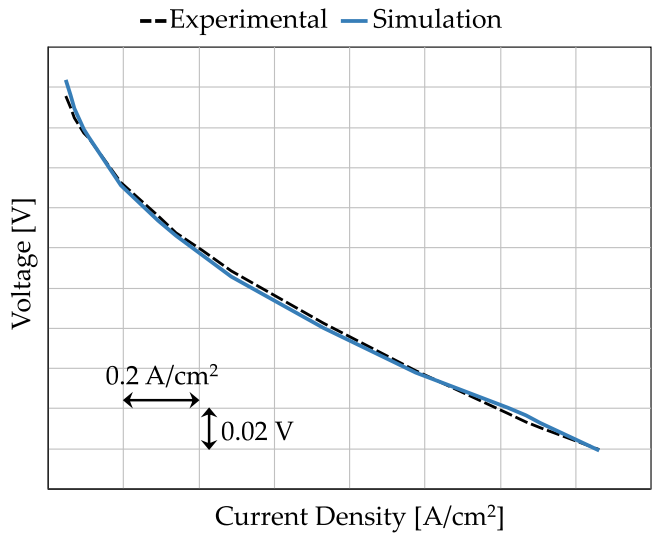


Fig. 3. Comparison between the simulated polarization curve and the experimental measurements over a single cell of the FC stack. Details on the FC current and voltage values are proprietary and, for this reason, labels have been removed from the axes.

Fig. 4(b) depicts the Stack (green) and BoP (red) efficiencies plotted as a function of current, with the relative percentage difference (gray line). The presence of the ancillaries in the BoP causes a drop in the system efficiency between 3%–15%, caused mainly by the compressor power consumption. In particular, the efficiency drop increases with higher current values, as the compressor has to send higher air mass flow rates to guarantee oxygen supply and facilitate water removal. When considering the degradation, the reduced efficiency will force the fuel cell to provide a higher current to maintain the same power output. As a result, the compressor's power consumption increases, further penalizing fuel consumption.

3.3. Fuel cell degradation model

Differently from the ICE, whose performance does not show any significant degradation with respect to lifetime, several studies demonstrate that the efficiency of an FC system decreases with increasing operating hours [25]. Thus, the EMS should be aware of the current state and the degradation rate of the FC to properly choose the best power split. Various physical phenomena lead to natural degradation during steady-state operation, but the FC degradation is more relevant in highly dynamic conditions [25]. In automotive applications, where load changes, start and stop, and cold start events are quite frequent, being able to capture the phenomena leading to degradation is particularly relevant in dynamic conditions. According to [71], the average stack efficiency can be estimated considering the cell voltage, as follows:

$$\eta_{FC} = \frac{V_{cell} - \Delta V_{cell}}{V_{th}} \tag{5}$$

where V_{cell} and V_{th} are the nominal and the theoretical FC voltage, while ΔV_{cell} is the voltage loss due to degradation. Since in this study experimental data in aged conditions were not available, a simplified approach derived from the methodology proposed in [38] was used for the voltage loss estimation:

$$\Delta V_{cell} = \int \Delta V_{LL}(i)\, dt + \int \Delta V_{LC}\left(\frac{di}{dt}\right) dt + \Delta V_{ss} \cdot n_{ss} \tag{6}$$

where:

- $\Delta V_{LL}(i)$ is the voltage decay due to the load level and is computed from the formulation derived from [38] rescaled to the actual FC current density (see black line in Fig. 6);
- ΔV_{LC} is the voltage decay for each load change which is formulated as follows:

$$\Delta V_{LC}\left(\frac{di}{dt}\right) = \Delta V_{LC}^{ref} \cdot \frac{\left|\frac{\Delta i(t)}{dt}\right|}{2\left|\frac{\Delta i_{ref}}{dt}\right|} \tag{7}$$

  where ΔV_{LC}^{ref} is the degradation introduced at a reference variation of current density Δi_{ref}, and $\Delta i(t)$ is the instantaneous current density variation. In this work, according to [38], $\Delta V_{LC}^{ref} = 6^{-7}$ μV/h and $\Delta i_{ref} = 0.99$ A/cm^2;
- ΔV_{ss} is the voltage decay for each on/off switching cycle and is measured in [V] and n_{ss} is the corresponding event frequency. In this work, according to [38], a constant voltage decay equal to 19.6 μV is considered for each start-up and shutdown event.

From a system point of view, the overall efficiency is given by:

$$\eta_{FC,S} = \eta_{FC}\eta_{aux}\eta_{DC/DC} \tag{8}$$

where η_{FC} is the stack efficiency, η_{aux} is the auxiliaries efficiency, and $\eta_{DC/DC}$ is the efficiency of the power converters. It should be noted that in this work the intrinsic dependency of η_{aux} on η_{FC} is considered: when the voltage of the FC decays, higher currents, and thus higher mass flow rates of air and hydrogen are necessary, which negatively affect η_{aux}.

4. Energy management strategies

In the hybrid powertrains, Conf.#2, #3, and #4, the ICE and the FC are the primary power sources, while the HV battery is an auxiliary one. For these configurations, an energy management strategy must be properly designed to optimize the power split between the power actuators.

Energy management in an HEV can be formalized as a constrained and finite-time optimal control problem [73] described by the state equation:

$$\dot{x}(t) = f(x(t), u(t), t) \tag{9}$$

where $x(t) \in \mathbb{R}^n$ and $u(t) \in \mathbb{R}^m$ are the state and control variables vector, t is the time variable, and f is a function modeling the dynamics of the system. To obtain an optimal contro law $u(t) : [t_0, t_f] \in \mathbb{R}^m$, the cost function must be minimized:

$$J = \phi\left(x(t_f), t_f\right) + \int_{t_0}^{t_f} L(x(t), u(t), t)\, dt \tag{10}$$

where $L(x(t), u(t), t) \in \mathbb{R}$ is the instantaneous cost function and $\phi\left(x(t_f), t_f\right) \in \mathbb{R}$ is the terminal cost incurred at the end of the process. In HEVs, L is typically the instantaneous fuel consumption, and the cost function J is subject to a set of both local and global constraints, i.e., physical limitations of the actuators and of the electrochemical battery.

In this work, the Equivalent Consumption Minimization Strategy (ECMS) [54] was chosen to address the described control problem. This strategy guarantees suboptimal performance and ease of implementation, thus allowing to obtain a fair comparison between the hybrid powertrains. The ECMS converts the global optimization problem formalized in Eqs. (9), and (10) into a local optimization problem. It instantaneously chooses the power split between the battery and the APU, i.e., ICE in Conf.#3 and FC in Conf.#4, that minimizes the overall H_2 consumption while respecting the battery SoC charge-sustaining constraint. The performance of the ECMS was assessed by comparing it with a Rule-Based (RB) control strategy previously implemented by the Authors in [53]. The RB strategy is easy to design and apply in a real system, but can rarely yield close-to-optimal solutions. Nevertheless, this strategy was used as a benchmark since it is the most common algorithm adopted in real vehicles. In fact, it represents a good compromise between satisfactory performance and ease of implementation in a vehicle Electronic Control Unit (ECU). More details about the two control strategies will be given in the following Sections.

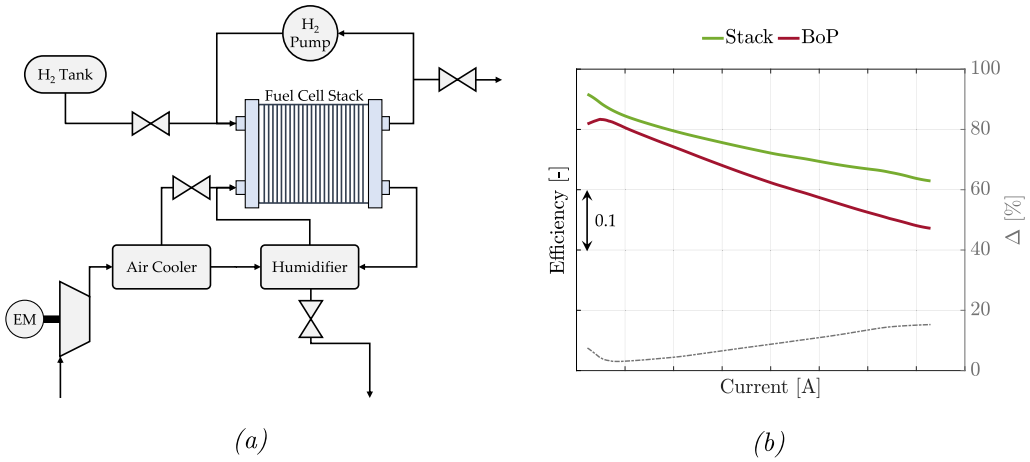


Fig. 4. (a) Schematic representation of the FC system along with all the ancillaries needed to guarantee its correct operation. (b) Stack (green) and BoP (red) efficiencies plotted as a function of current, with the relative percentage difference (gray line). Details on the exact efficiency values are proprietary and, for this reason, labels have been removed from the axis.

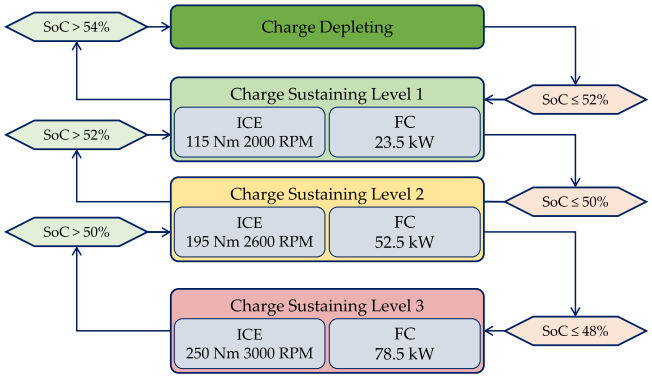


Fig. 5. Rule-based strategy logic showing powertrains operation levels based on State of Charge (SoC).

4.1. RB

For both powertrain configurations, the implemented heuristic approach features three charging levels: 23.5 kW, 52.5 kW, and 78.5 kW. The transitions among these levels are governed by the battery SoC. For clarity, Fig. 5 shows a flow chart that describes the charging levels and their corresponding conditions. Additionally, the control strategy includes some constraints that avoid operating conditions close to the full load curve and to reduce the thermal and mechanical stresses on the engine components. Similarly, the charging levels are well-suited also for the FC system. In particular, the first level enables operation near a high efficiency region, while the third level avoids full power helping to minimize the FC degradation rates.

4.2. ECMS

The ECMS is a static control strategy that relies on the instantaneous optimization of the powertrain energy flows to achieve sub-optimal results while being feasible in a vehicle ECU [74]. In this formulation, an equivalent fuel consumption, $\dot{m}_{f,eq}(t)$ is obtained by summing $\dot{m}_{f,i}(t)$, the fuel consumption of ICE or FC in Conf.#3 and #4, respectively, to $\dot{m}_{el}(t)$ a "virtual" fuel consumption related to the use of the battery. The equivalent fuel consumption is instantaneously minimized as follows:

$$\dot{m}_{f,eq}(t) = \dot{m}_{f,i}(t) + \frac{s(t)P_{batt}(t)}{Q_{LHV}}, \quad i \in \{ICE, FC\} \tag{11}$$

where $P_{batt}(t)$ is the instantaneous power provided or absorbed by the battery; Q_{LHV} is the fuel's lower heating value; $s(t)$ is the instantaneous equivalence factor converting the battery energy consumption into the virtual fuel consumption. However, in order to obtain sub-optimal results, this approach requires the adoption of the appropriate value of equivalence factor $s(t)$, which depends on both the powertrain topology and the specific mission profile [75]. For obtaining the equivalence factors, the design optimizer integrated in GT-SUITE® was used in this work. It relies on a genetic algorithm that selects the equivalence factor value minimizing the difference between initial and final SoC values. Although the ECMS requires the a-priori tuning of the equivalence factor, this strategy may be considered appropriate for this application as an urban bus always follows the same route, and thus encounters repetitive driving patterns.

The ECMS requires the selection of one or more independent variables, namely the control variables, that are discretized to create feasible scenarios. The ECMS, then, chooses the scenario that minimizes the equivalent fuel consumption from among them. Since, in a series HEV, the ICE is disconnected from the wheels, it is possible to optimize the engine operation both in terms of speed and torque. For these reasons, the developed ECMS for Conf.#3 incorporates two control variables, i.e., ICE speed and power, discretized with resolutions of 150 RPM, and 2 kW, respectively. The ECMS developed for Conf.#4, instead, includes only one control variable, i.e., FC power, discretized with a resolution of 1 kW.

4.3. ECMS w/deg

As already outlined in Section 1, the EMS of an FCEV should also consider FC aging to guarantee long-lasting operation and thus reach competitiveness, in particular in terms of TCO, with other technologies. In this work, the three main factors that contribute to FC degradation, described in Section 3.3, are curbed through the following conditions:

- Load Level (ΔV_{LL}):
  The classical ECMS formulation was modified to reduce the degradation coming from load level by adding a term that is related to the FC degradation:

$$\dot{m}_{f,eq}(t) = \dot{m}_{f,FC}(t) + \frac{s(t)P_{batt}(t)}{Q_{LHV}} + \dot{m}_{deg,FC}(t) \tag{12}$$

  where $\dot{m}_{deg,FC}(t)$ is the component that takes into account the degradation coming from load level and is formulated as follows:

$$\dot{m}_{deg,FC}(t) = \begin{cases} 0 & \text{if } I < I_P \\ k * (I - I_P) & \text{if } I \geq I_P \end{cases} \tag{13}$$

  and I_P and k are calibration factors that were properly tuned through a sensitivity analysis. The effect of the penalty can be

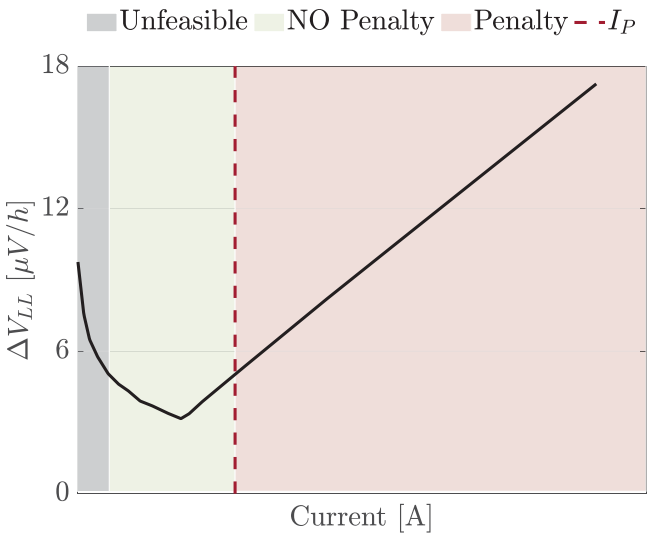


Fig. 6. Degradation due to load level as a function of current along with the different regions defined in the ECMS$_{w/deg}$ formulation marked by different colors. The unfeasible, not penalized, and penalized areas are represented in gray, green, and pink, respectively. Details on the FC current values are proprietary and, for this reason, labels have been removed from the x-axis. (For interpretation of the references to color in this figure legend, the reader is referred to the web version of this article.)

more clearly understood from Fig. 6, where the share of FC degradation coming from load level is plotted as a function of FC current. Details on the FC current values are proprietary and, for this reason, labels have been removed from the x-axis. It is worth noting that the degradation (see Section 3.3) initially decreases exponentially with the current, and, after reaching the minimum, increases linearly. The control system was configured in order to freely choose the best current in the region with less degradation (green area). Excessively small current values (gray area in the plot) are avoided as this would lead to both high degradation and low efficiencies. On the other hand, the $\dot{m}_{deg,FC}(t)$ penalty (see Eq. (12)) is added to the ECMS formulation only for $I > I_P$ (pink area in the plot), featuring a linear correlation with current to resemble the degradation trend.

- Load Change (ΔV_{LC}):
  For limiting the degradation due to load change, the maximum allowable variation of di/dt was imposed equal to 0.01 A/cm^{2}s. This condition may seem extremely conservative (see [38]) but it allows for maximizing FC lifetime. On the other hand, increasing the dynamic limitations may penalize the FC flexibility, preventing the control strategy from keeping the charge-sustaining mode in aggressive and high-power driving conditions. Therefore, the controller was allowed to bypass the limits imposed in terms of di/dt if P_{driver} > 150 kW or SoC < 0.3.
- Start & Stop:
  Since the start/stop strongly affects the aging of the FC, the control strategy keeps the FC always on during the entire simulation;

For the sake of clarity, hereinafter the standard ECMS will be referred to as ECMS, while the modified version of the ECMS (featuring the penalty factor) as ECMS$_{w/deg}$.

5. Simulation results

The virtual test rig of the 12 m bus was used to assess the energy consumption of the powertrain configurations listed in Table 2 on the selected mission profiles. Since this work aims to provide a fair comparison between H_2-fueled powertrains for urban buses application, this Sections will be mainly focused on these configurations. In particular, this Section is divided into four different subsections. Section 5.1 summarizes the assumptions that were made for considering the effect of auxiliaries and passengers on the bus energy consumption. Sections 5.2 and 5.3 focus on the energy consumption of Conf.#3 and #4, respectively. For the sake of brevity, the results will be shown more in detail only on the Braunschweig driving cycle, while the other two cycles will be used to make a comparison in terms of fuel economy and FC degradation. Finally, Section 5.4 assesses the energy consumption of the H_2-fueled powertrains by benchmarking them against Conf. #1,#2, and #5.

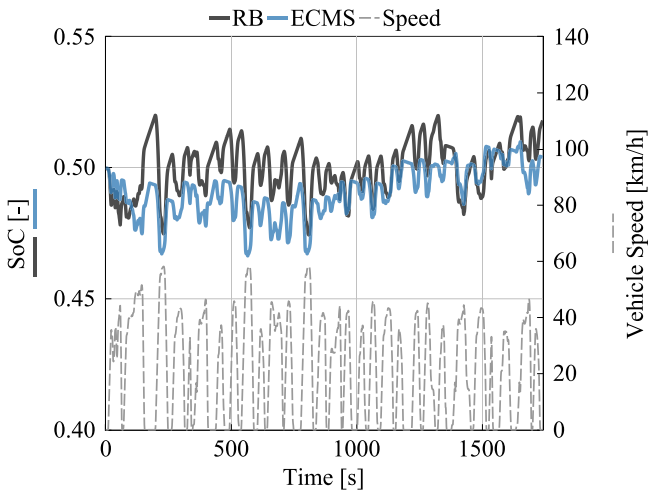


Fig. 7. Conf.#3: SoC as a function of time for the RB (gray) and the ECMS (blue) on the Braunschweig driving cycle. (For interpretation of the references to color in this figure legend, the reader is referred to the web version of this article.)

5.1. Assumptions

It is noteworthy to mention that, when comparing HDVs to passenger cars, the energy consumption of the auxiliaries has a bigger effect on the total energy consumption. This rings particularly true for BEVs, where extreme weather conditions can even double the bus energy consumption when compared to moderate weather conditions [76], which, therefore, significantly reduces its driving range. In order to perform a technology-neutral comparison, in this work the following assumption was made: the bus operates in an environmental temperature range of 15–20 °C, in which, according to [76], the power absorption due to Heating, Ventilation, and Air Conditioning (HVAC) and battery thermal management is limited (about 1 kW). Moreover, in line with the values reported in [76,77] for the abovementioned conditions, the power absorption of the bus auxiliaries (i.e., air compressor, steering pump, suspension system, etc.) is imposed equal to 1.35 kW. Finally, the weight of the passengers cannot be neglected in a bus application as it can drastically increase the gross weight of the vehicle. Thus, for the sake of consistency, passengers' load is held constant across the different simulations and is fixed at 54 passengers (60% occupancy rate), each weighing 72.85 kg (average gender-neutral weight in Italy).

5.2. Conf.#3: H2-HEV

In this section, the results of the Conf.#3 will be analyzed and the results of the developed ECMS control logic will be compared with the RB strategy. In Fig. 7 the SoC profiles of the RB strategy (gray) and of the ECMS logic (blue) are plotted as a function of time. It should be noted that, although both strategies reach the final charge sustainability, their behavior is visibly different. While the RB strategy follows periodic SoC variations, the ECMS tends to mainly discharge and then recharge the battery.

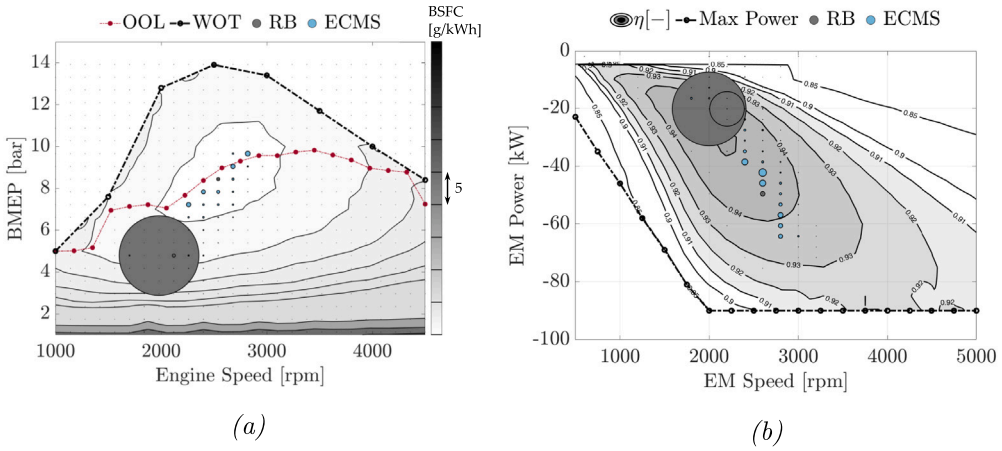


Fig. 8. Conf.#3: Time distribution for the RB (gray) and the ECMS (blue) on the Braunschweig driving cycle. (a) H_2-engine on the BSFC map; (b) EM on the efficiency map. (For interpretation of the references to color in this figure legend, the reader is referred to the web version of this article.)

Table 5
Conf.#3: Comparison in terms of final SoC (SoC_f) and Fuel Economy (FE) over the Braunschweig, Gillingham, and MLTB driving cycles for the RB and the ECMS.

			RB	ECMS	
Braunschweig	FE	[g/km]	85.0	78.7	−7.5%
	SoC_f	[−]	0.518	0.504	−2.6%
Gillingham	FE	[g/km]	96.3	91.0	−5.5%
	SoC_f	[−]	0.521	0.503	−3.5%
MLTB	FE	[g/km]	84.1	80.2	−4.6%
	SoC_f	[−]	0.506	0.502	−0.7%

Additional considerations can be done from Fig. 8, where the time distribution of the engine operating points is reported on its engine Brake Specific Fuel Consumption (BSFC) map: the larger the circle, the higher the time spent by the engine in that operating zone. The red dotted line represents the Optimal Operating Line (OOL), i.e., the line that links the highest efficiency points at fixed engine rotational speeds, while the black dotted line represents the Wide Open Throttle (WOT) curve, i.e., the maximum BMEP at fixed engine rotational speeds. Details on the BSFC values are proprietary and, for this reason, labels have been removed from the contour lines. While the RB makes the engine work mainly in one operating point defined by the set of rules, the optimization performed by the ECMS allows the engine to work almost entirely in the most efficient region, close to the OOL line.

The different engine operation, obtained by the EMCS, enhances its fuel economy in comparison to the RB as can be seen from Fig. 9, where the trade-off between fuel economy and final SoC values is shown, and from Table 5 where the corresponding numerical values are displayed. For the considered driving cycles, represented with a specific symbol, i.e., circle, rhombus, and square, for Braunschweig, Gillingham, and MLTB, respectively, the ECMS improves the fuel economy by about 5.9% on average, if compared to the RB strategy. It is noteworthy to mention that, although the discrepancy in terms of final SoC values between the two strategies may appear quite significant (from 0.4% to 1.8%), it is instead quite limited if compared to the energy required during the entire driving cycle, i.e., less than 0.35 kWh over a total energy request of 25–50 kWh (considering all the three driving cycles), which corresponds to less than 1%.

5.3. Conf.#4: FCEV

In this section, Conf.#4 will be analyzed and the results of the developed ECMS control logic will be assessed against the RB strategy. Differently from Conf.#3, the modified version of the ECMS that takes

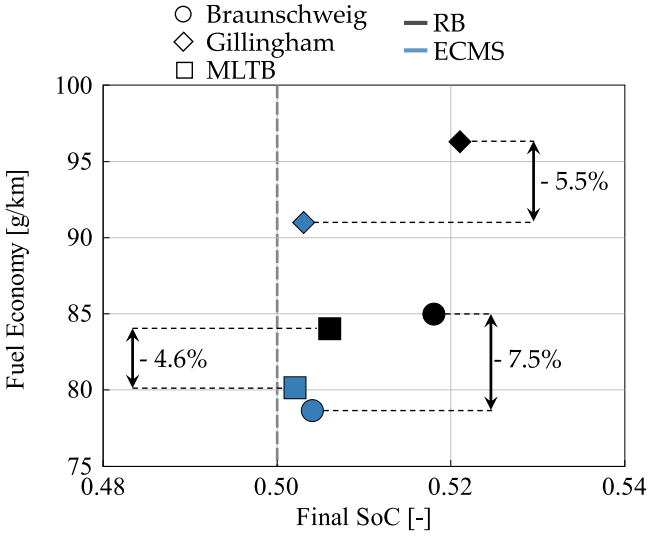


Fig. 9. Conf.#3: Comparison of the results over the Braunschweig (circle), Gillingham (rhombus), and MLTB (square) driving cycles for the RB (gray) and ECMS (blue): trade-off between fuel economy and final SoC values. (For interpretation of the references to color in this figure legend, the reader is referred to the web version of this article.)

into account FC degradation ($ECMS_{w/deg}$) will be also analyzed. In the upper plot of Fig. 10 the SoC profiles of the RB (gray), the ECMS (blue), and $ECMS_{w/deg}$ (red) strategies are plotted as a function of time on the Braunschweig driving cycle. Details on the FC current values are proprietary and, for this reason, labels have been removed from its axis. Similarly to Conf.#3, all the strategies reach the final charge sustainability, but the control laws are clearly different. While the RB strategy follows periodic SoC variations, the ECMS tends to discharge and then charge the battery. The $ECMS_{w/deg}$, instead, features wider oscillations reaching lower SoC values. The differences among the three control strategies can be more clearly observed in the middle plot of Fig. 10, where the FC current profiles are plotted as a function of time. As expected, the RB strategy makes the RB provide only three values of current (corresponding to the charging levels). Comparing the ECMS and $ECMS_{w/deg}$, it can be seen that the proposed $ECMS_{w/deg}$ controls the current of the FC system less dynamically than the reference ECMS. The constraints imposed on the $ECMS_{w/deg}$ strongly limit the current swings if compared to the standard ECMS, and make it work, whenever possible, at constant current.

Table 6
Conf.#4: Comparison in terms of final SoC (SoC_f) and Fuel Economy (FE) over the Braunschweig, Gillingham, and MLTB driving cycles for the RB, ECMS, and $ECMS_{w/deg}$. The percentage reductions are expressed relative to RB.

			RB	ECMS		$ECMS_{w/deg}$	
Braunschweig	FE	[g/km]	55.8	52.8	−5.4%	54.1	−3.1%
	SoC_f	[−]	0.513	0.499	−2.6%	0.496	−3.3%
Gillingham	FE	[g/km]	68.0	65.3	−4.0%	65.0	−4.5%
	SoC_f	[−]	0.525	0.500	−4.7%	0.492	−6.3%
MLTB	FE	[g/km]	56.7	52.3	−7.8%	53.5	−5.6%
	SoC_f	[−]	0.509	0.498	−2.1%	0.499	−1.9%

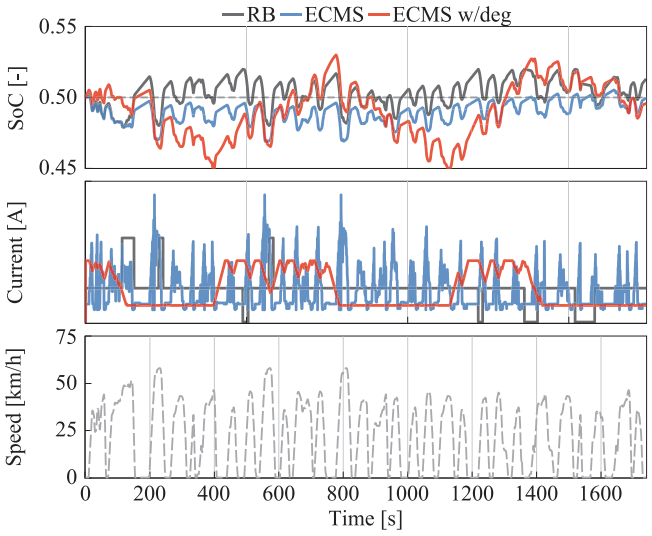


Fig. 10. Conf.#4: Battery SoC (upper plot), FC current (middle plot), and vehicle speed profile (bottom plot) plotted as a function of time for the RB (gray), the ECMS (blue), and the $ECMS_{w/deg}$ (red) on the Braunschweig driving cycle. Details on the FC current values are proprietary and, for this reason, labels have been removed from its axis. (For interpretation of the references to color in this figure legend, the reader is referred to the web version of this article.)

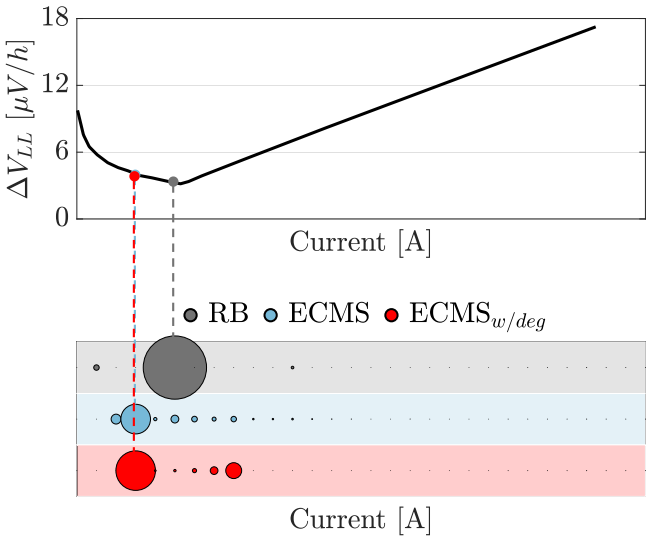


Fig. 11. Conf.#4: Current time distribution on the degradation curve due to load level for the RB (gray), the ECMS (blue), and the $ECMS_{w/deg}$ (red) on the Braunschweig driving cycle. Details on the FC current values are proprietary and, for this reason, labels have been removed from its axis. (For interpretation of the references to color in this figure legend, the reader is referred to the web version of this article.)

Some additional considerations can be done from Fig. 11 where the current time distribution of the FC operating points is reported under the FC degradation curve: the larger the circle on the colored bands representing the strategies, the higher the time spent by the FC in providing the current on the x-axis. For the RB strategy (gray), the FC virtually works in one operating point (the constant value of current that is also visible in Fig. 10) corresponding to a very low value of degradation. The ECMS (blue) and the $ECMS_{w/deg}$ (red), instead, have some similarities: although Fig. 10 showed completely different current trends, Fig. 11 proves that their time distributions do not differ excessively as the bigger circles of the two strategies are virtually vertically aligned.

As already done for Conf.#3, further considerations can be done also for Conf.#4 from Fig. 12, where the trade-off between fuel economy and final SoC values is shown, and from Table 6 where the corresponding numerical values are displayed. The $ECMS_{w/deg}$ improves the fuel economy by about 4.4% on average, if compared to the RB strategy. Moreover, although the conditions introduced in the $ECMS_{w/deg}$ limit its freedom to minimize the overall fuel consumption, they do not excessively penalize the FC fuel economy if compared to the standard ECMS (+1.4% on average). It is worth noting that, by comparison with the standard ECMS, the slightly better fuel economy of the $ECMS_{w/deg}$ on the Gillingham driving cycle is only due to the slightly lower value of the final SoC. Finally, regarding the discrepancy in terms of final SoC values between the three strategies and the overall requested energy, similar considerations apply to those expressed for Conf.#3.

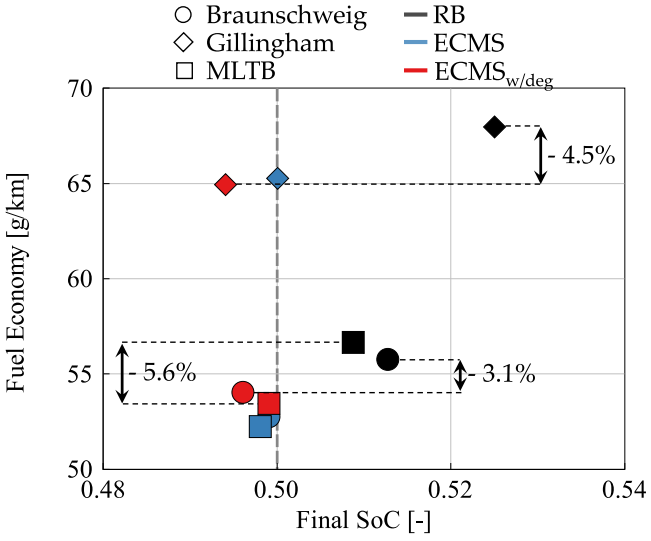


Fig. 12. Conf.#4: Comparison of the results over the Braunschweig (circle), Gillingham (rhombus), and MLTB (square) driving cycles for the RB (gray), ECMS (blue), and $ECMS_{w/deg}$ (red): trade-off between fuel economy and final SoC. (For interpretation of the references to color in this figure legend, the reader is referred to the web version of this article.)

The effect of the different control strategies in terms of FC degradation can be seen in Fig. 13, where the contributions coming from

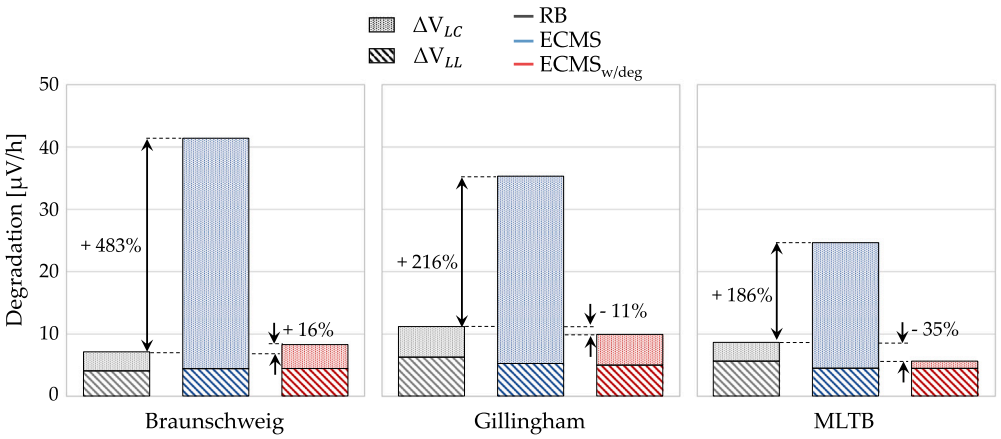


Fig. 13. Conf.#4: Graphical comparison of the different factors contributing to FC degradation over the Braunschweig, Gillingham, and MLTB driving cycles for the RB (gray), ECMS (blue), and ECMS$_{w/deg}$ (red). (For interpretation of the references to color in this figure legend, the reader is referred to the web version of this article.)

Table 7
Conf.#4: Numerical comparison of the different factors contributing to FC degradation over the Braunschweig, Gillingham, and MLTB driving cycles for the RB, ECMS, and ECMS$_{w/deg}$. The values are expressed in [μV/h].

		RB	ECMS	ECMS$_{w/deg}$
Braunschweig	Load Level	4.0	4.4	4.4
	Load Change	3.1	37.1	3.9
	Total	7.1	41.5	8.3
Gillingham	Load Level	6.3	5.2	5.0
	Load Change	4.9	30.2	4.9
	Total	11.2	35.4	9.9
MLTB	Load Level	5.6	4.5	4.4
	Load Change	3.0	20.2	1.2
	Total	8.6	24.7	5.6

load level (pattern with diagonal lines) and load change (pattern with small dots) and represented on a bar plot. It is worth noticing that, while the degradation due to the load level is similar between the three strategies, the one deriving from the load change is drastically different. This result could already have been inferred by observing Fig. 10: the RB features simple rules, and the current is kept constant for long time intervals, leading to a low degradation level, but a fuel economy far from the optimum. The standard ECMS obtains a much better fuel economy (see Fig. 12) but at the expense of higher degradation due to the continuous load changes. In fact, the optimizer instantaneously selects the power split that minimizes the equivalent fuel consumption but does not take into account the degradation of the FC. Lastly, the ECMS$_{w/deg}$, thanks to the introduction of the additional conditions, allows for drastically limiting the degradation of the FC without jeopardizing the fuel economy (comparable with standard ECMS). It is worth noting that, on the Braunschweig driving cycle, the ECMS$_{w/deg}$ presents higher values of degradation if compared to the RB strategy. In this cycle, the RB strategy makes the FC work on the same operating point for almost the entire driving cycle, which results in a remarkably low FC degradation coming from load change. More granularity is given by Table 7 where the numerical comparison between the FC degradation obtained on all the driving cycles is listed for the different control strategies. It should be noted that, on the Gillingham and MLTB driving cycles, the ECMS$_{w/deg}$ allows for reducing the degradation of the FC if compared to the RB strategy.

A further analysis was performed to estimate the effect that each control strategy has on the FC life expectancy. The end-of-life was conventionally set when the FC system reached 40% of its initial efficiency, which is in line with the condition established by the U.S. Department of Energy of 10% voltage drop at a current density of 1 A/cm^2 [78]. The FC life, in terms of km, was estimated by advancing the simplistic assumption that the FCEV covered always the same mission profile during its entire life. The values reported in Table 7 were substituted into Eqs. (5) and (6) to evaluate the contribution of load change and load level to efficiency and degradation rate. On the three control strategies, the same hypothesis was advanced for the on/off switching events: the FC was kept always on during the bus operation and shut off only at the end of a working day (conventionally set at 8 h). Fig. 14 shows the FC system efficiency plotted as a function of its lifetime (expressed in 10^3 km) in the case in which the Braunschweig driving cycle is iteratively repeated until the FC system reaches its end-of-life (depicted with a diamond marker). As already remarked, the simple rules of the RB allow extending the FC life but at the expense of higher fuel consumption. On the contrary, the ECMS strategy, while improving the FC fuel economy (see Fig. 12), drastically reduces its life expectancy due to the excessive load changes. Lastly, the ECMS$_{w/deg}$ can achieve values of life expectancy comparable to the RB strategy, without jeopardizing the fuel economy. It is worth mentioning that, as the system efficiency depends on the FC voltage, the slight differences observed in the system efficiency at the beginning of its life (see blue circle) can be attributed to variations in the operation of the control strategies.

More granularity is provided by Table 8 where the FC life, in terms of km, is shown for all the driving cycles. In line with what was seen in Fig. 14, the ECMS strategy drastically reduces the FC life expectancy also when the bus performs the other two driving cycles. This can be mainly attributed to the significant load variations introduced by this strategy. On the Gillingham and MLTB, instead, the ECMS$_{w/deg}$ does not only remarkably extend the FC life if compared to the standard ECMS, but is also able to slightly extend the FC life if compared to the RB strategy.

5.4. Tank-to-wheel analysis

The final section of this paper aims to provide a comparison between the two proposed hybrid H_2-fueled powertrains. Moreover, the viability of the H_2-fueled powertrains is assessed through a TTW analysis by benchmarking them against the other configurations listed in Table 2. Fig. 15 shows their energy consumption on the three considered driving cycles, where the reported values represent the primary energy consumption at fuel and battery levels, accounting for the efficiency losses at the powertrain level. The corresponding numerical values are displayed in Table 9, which also reports the percentage reduction from the ICEV for each configuration. Concerning the energy management of the hybrid powertrains, Conf.#2 and #3 feature a standard ECMS (see Section 5.2), while Conf.#4 features the ECMS$_{w/deg}$ (see Section 5.3). It is worth restating that the degradation of the FC

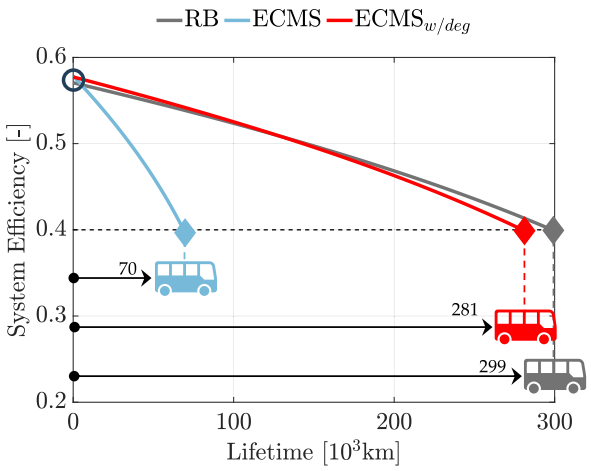


Fig. 14. Conf.#4: FC system efficiency plotted as a function of its lifetime (expressed in 10^3 km) over the Braunschweig driving cycle iteratively repeated until the FC system reaches its end-of-life for the RB (gray), ECMS (blue), and ECMS$_{w/deg}$ (red). (For interpretation of the references to color in this figure legend, the reader is referred to the web version of this article.)

Table 8
FC life, expressed in 10^3 km, estimated by advancing the assumption that the FCEV performs, during its entire life, always the same mission profile, and its end-of-life is conventionally set when the FC system reaches 40% of its initial efficiency.

	RB	ECMS	ECMS$_{w/deg}$
Braunschweig	299	70	281
Gillingham	204	75	222
MLTB	175	74	247

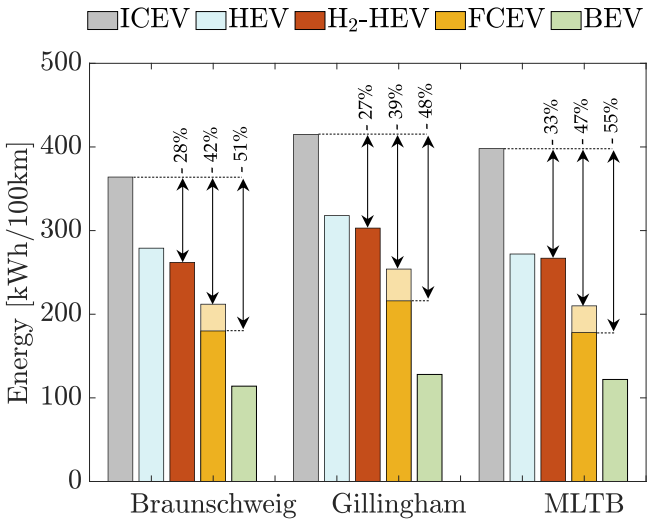


Fig. 15. Comparison of the energy consumption of the different powertrain configurations on the simulated driving cycles. Percentage reductions of H_2-fueled powertrains are expressed compared to ICEV. (For interpretation of the references to color in this figure legend, the reader is referred to the web version of this article.)

does not only affect its lifetime but also its fuel consumption [79,80]. Therefore, two different cases have been considered to take into account the effect that FC degradation has on energy consumption increase: FCEV$_1$ and FCEV$_2$ feature the energy consumption of the FC averaged over its lifetime and at the start of its life, respectively.

Analyzing Fig. 15, it can be noted that powertrain hybridization can significantly improve the fuel economy of a diesel bus (on average by 26%). In fact, despite widespread on the market, urban buses equipped with a large displacement diesel engine are characterized by high fuel consumption. Urban transit applications comprise continuous start-and-stop and driving patterns at low average speeds, which make the ICE work at efficiencies far from the optimum. Moving to a series-hybrid configuration with a downsized diesel engine not only allows for decoupling the ICE from the wheels, thus avoiding the idling during the stop phases and shifting the engine operations toward more efficient zones but also introduces the additional gains derived from regenerative braking, which are especially remarkable for an HDV such as an urban bus. The benefits introduced by hybridization are particularly pronounced on the MLTB driving cycle since it is characterized by the lowest average speed and the highest share of stop phases among the three driving cycles (see Table 4). The transition from diesel to hydrogen as a fuel not only allows to potentially decarbonize the urban bus but also to further reduce energy consumption (on average by 29% with reference to the ICEV). Substituting the ICE with an FC allows a further reduction of the energy consumption (on average by 51% with reference to the ICEV), but has fewer advantages on the Gillingham driving cycle since the FC performance worsens with more dynamic conditions and at higher loads. Considering the effect of FC aging (lighter yellow bar), the performance of the FC is hindered by its degradation. Despite the smaller gap with the H_2-HEV, it is still not zero, and the FCEV allows for reducing the energy consumption on average by 42% if compared to the ICEV. Finally, as expected, the BEV configuration can obtain the lowest energy consumption on a TTW basis (an average reduction of 69%, if compared to the ICEV).

Table 9
Comparison of the energy consumption, expressed in [kWh/100km], of the different powertrain configurations on the simulated driving cycles. FCEV$_1$ and FCEV$_2$ feature the energy consumption of the FC averaged over its lifetime and at the start of its life, respectively. For each configuration, the percentage reduction is expressed compared to the ICEV.

	ICEV	HEV	H_2-HEV	FCEV$_1$	FCEV$_2$	BEV
Braunschweig	364	279	262	212	180	114
		−23%	−28%	−42%	−51%	−69%
Gillingham	415	318	303	254	216	128
		−23%	−27%	−39%	−48%	−69%
MLTB	398	272	267	210	178	122
		−32%	−33%	−47%	−55%	−69%

It should be restated that Fig. 15 compares the different powertrains only based on a TTW approach, not considering the energy consumption and the CO_2 emissions produced in the Well-to-Tank (WTT) phase, and therefore may not represent a comprehensive comparison [81]. A LCA, instead, would allow for quantifying the emissions generated throughout the entire vehicle life, by including vehicle and powertrain production, vehicle use, and end-of-life disposal, as well as emissions generated during the production and the transport of the energy vectors. However, accurate estimation of powertrain energy consumption is of paramount importance for conducting a robust LCA. The meticulous modeling of the H_2 powertrains establishes a solid foundation for an LCA analysis grounded in realistic and reliable data. Consequently, in future works, we will leverage the findings of this study to allow a more in-depth comparison of the different powertrain configurations through LCA, providing a comprehensive quantification of emissions generated throughout the life cycle of the vehicle.

6. Conclusions and further developments

In this study we performed a detailed theoretical investigation on the use of H_2-fueled powertrains as possible pathways to reduce the carbon footprint of a 12 m urban bus. Each of the two hybrid H_2-fueled powertrains, namely a H_2-Internal Combustion Engine (ICE) and a Fuel Cell (FC), was carefully modeled and validated against experimental data or through detailed 1D–3D CFD simulations.

In order to obtain a fair comparison, we devoted particular attention to the development of control strategies tailored for H_2-fueled powertrains. A standard Equivalent Consumption Minimization Strategy

(ECMS) was proposed for the H_2-HEV, while a modified version of the ECMS ($ECMS_{w/deg}$) was tailored for the FCEV to minimize its fuel consumption and maximize its lifetime.

Finally, we provided a comparison between the two proposed H_2-fueled propulsion systems based on a Tank-to-Wheel (TTW) approach. In this analysis, other technologies available in the market are used as a benchmark: a conventional Internal Combustion Engine (ICE) vehicle, a diesel HEV, and a Battery Electric Vehicle (BEV). The simulation results proved that the hybrid H_2-fueled powertrains cannot only decarbonize a diesel ICE bus but also reduce its energy consumption by an average of 29% (H_2-HEV), and 42% (FCEV).

The detailed H_2-fueled powertrain investigation allowed us to conclude that:

- Both H_2-fueled powertrains represent valid pathways to decarbonize urban bus fleets. They also allow to reduce the energy consumption of a diesel ICE bus by an average of 29% (H_2-HEV), and 42% (FCEV);
- This study achieved an accurate estimation of powertrain energy consumptions, which is of paramount importance for a subsequent and more comprehensive Life Cycle Assessment (LCA);
- A fair comparison between FCEV and H_2-ICEV should also take into account FC degradation; simulations have shown that a well-designed energy management strategy could extend the FC life by more than three times if compared to a standard one;
- By directly comparing the H_2-fueled powertrains, the FCEV allows to reduce on average the energy consumption of the bus by 19% if compared to the H_2-HEV. Therefore, on a TTW basis, the FC can achieve better fuel economy than a H_2-ICE. However, considering the FC aging in the fuel economy comparison reduces the gap between the H_2-fueled powertrains. This makes also the H_2-HEV a valid alternative for urban bus applications.

Finally, since the energy consumption of the auxiliaries can significantly increase the fuel consumption of Heavy Duty Vehicles (HDVs) – extreme weather conditions can even double the energy consumption of a battery electric bus when compared to moderate weather conditions – future work will consider the effect of additional weather scenarios in the comparison between the powertrain configurations. Finally, future work will consider also the battery state of health in the energy management strategy of the hybrid powertrains.

Abbreviations

The following abbreviations are used in this manuscript:

APU	Auxiliary Power Unit
BEV	Battery Electric Vehicle
BMEP	Brake Mean Effective Pressure
BoP	Balance of Plant
BSFC	Brake Specific Fuel Consumption
CV	Conventional Vehicle
ECMS	Equivalent Consumption Minimization Strategy
ECU	Electronic Control Unit
EM	Electric Machine
EMS	Energy Management System
FC	Fuel Cell
FE	Fuel Economy
FCEV	Fuel Cell Electric Vehicle
GHG	Greenhouse Gas
HDV	Heavy-Duty Vehicle
HEV	Hybrid Electric Vehicle
HVAC	Heating, Ventilation, and Air Conditioning
ICE	Internal Combustion Engine
ICEV	Internal Combustion Engine Vehicle
LCA	Life-Cycle Assessment
LDV	Light-Duty Vehicle
LFP	Lithium Iron Phosphate
MLTB	Millbrook London Transport Bus
NCM	Nickel–Cobalt–Manganese
OCV	Open Circuit Voltage
OOL	Optimal Operating Line
PID	Proportional–Integral–Derivative
PM	Permanent Magnet
RB	Rule-Based
RBS	Regenerative Braking System
SoC	State of Charge
TTW	Tank-To-Wheel
WOT	Wide Open Throttle
WTT	Well-to-Tank
ZEV	Zero-Emissions Vehicle

Symbols

The following symbols are used in this manuscript:

CO_2	carbon dioxide
f	function modeling the dynamics of the system
F	Faraday constant
k	calibration factor
i	current density
I	current
i_L	limiting current
I_P	current penalization
i_0	exchange current density
$i_{0,ref}$	reference exchange current density
J	cost function
$L(x(t), u(t), t)$	instantaneous cost function
$\dot{m}_{deg,FC}(t)$	equivalent fuel consumption due to degradation
$\dot{m}_{f,ICE}(t)$	ICE fuel consumption
$\dot{m}_{f,FC}(t)$	FC fuel consumption
$\dot{m}_{f,eq}(t)$	equivalent fuel consumption
NO_x	nitrogen oxides
n	number of electrons involved
n_{ss}	on/off switching frequency
$P_{batt}(t)$	instantaneous battery power
P_{driver}	power required by the driver
Q_{LHV}	fuel lower heating value
R	universal gas constant
R_i	internal resistance
$s(t)$	instantaneous equivalence factor
t	time variable
T	temperature
$u(t)$	control variable
$x(t)$	state variable
V_{act}	loss associated to electrochemical reaction
V_{cell}	nominal FC voltage
V_{conc}	concentration loss
V_{ocv}	OCV at null current
V_{ohm}	loss associated to protonic conductivity
V_{th}	theoretical FC voltage
Δi_{ref}	reference variation of current density
ΔV_{cell}	voltage loss due to degradation

$\Delta V_{LL}(i)$	voltage decay due to the load level
ΔV_{LC}	voltage decay for each load change
ΔV_{LC}^{ref}	degradation introduced at a reference variation of current density
ΔV_{ss}	voltage decay for each on/off switching cycle
α	charge transfer coefficient
η_{aux}	auxiliaries efficiency
$\eta_{DC/DC}$	efficiency of the power converters
η_{FC}	average stack efficiency
$\eta_{FC,S}$	overall system efficiency
$\phi\left(x(t_f), t_f\right)$	terminal cost

CRediT authorship contribution statement

Luca Pulvirenti: Writing – original draft, Validation, Software, Methodology, Formal analysis, Conceptualization. **Luciano Rolando:** Writing – review & editing, Supervision, Project administration, Methodology, Formal analysis, Conceptualization. **Afanasie Vinogradov:** Writing – review & editing, Software, Methodology, Formal analysis, Conceptualization. **Benedetta Peiretti Paradisi:** Writing – review & editing, Methodology, Conceptualization.

Declaration of competing interest

The authors declare that they have no known competing financial interests or personal relationships that could have appeared to influence the work reported in this paper.

Acknowledgments

This work was supported by Ministero dell'Università e della Ricerca (MUR) in the framework of PRIN2020. Project Title: Development of a Hydrogen Fueled Hybrid Powertrain for Urban Buses. Grant number: 2020R92Y3Z.

References

[1] IEA. Largest end uses of energy by sector in selected IEA countries, 2019. 2022, https://www.iea.org/data-and-statistics/charts/largest-end-uses-of-energy-by-sector-in-selected-iea-countries-2019. online documentation.

[2] EEA. Greenhouse gas emissions from transport in Europe. 2022, https://www.eea.europa.eu/ims/greenhouse-gas-emissions-from-transport. online documentation.

[3] ACEA. Fact sheet: CO2 standards for heavy-duty vehicles. 2023, https://www.acea.auto/fact/fact-sheet-co2-standards-for-heavy-duty-vehicles/. online documentation.

[4] UNECE. European Green deal: Commission proposes transformation of EU economy and society to meet climate ambitions," accessed october 2021. 2021, https://ec.europa.eu/commission/presscorner/detail/en/IP_21_3541. online documentation.

[5] Commission E. Proposal for a regulation of the european parliament AND of the council amending regulation (EU) 2019/1242 as regards strengthening the CO2 emission performance standards for new heavy-duty vehicles and integrating reporting obligations, and repealing regulation (EU) 2018/956. 2019, https://eur-lex.europa.eu/legal-content/EN/TXT/?uri=COM:2023:88:FIN. online documentation.

[6] Zhang C, Zhao X, Sacchi R, You F. Trade-off between critical metal requirement and transportation decarbonization in automotive electrification. Nat Commun 2023;14(1):1616. http://dx.doi.org/10.1038/s41467-023-37373-4.

[7] Çabukoglu E, Georges G, Küng L, Pareschi G, Boulouchos K. Battery electric propulsion: An option for heavy-duty vehicles? Results from a swiss case-study. Transp Res Part C: Emerg Technol 2018;88:107–23. http://dx.doi.org/10.1016/j.trc.2018.01.013.

[8] Garcia A, Monsalve Serrano J, Sari RL, Tripathi S. Life cycle CO2 footprint reduction comparison of hybrid and electric buses for bus transit networks. Appl Energy 2022;308:118354. http://dx.doi.org/10.1016/j.apenergy.2021.118354.

[9] EU. Hydrogen roadmap Europe: A sustainable pathway for the European energy transition. Publications Office; 2019, http://dx.doi.org/10.2843/341510.

[10] Zhang X, Zhou Y. Life-cycle carbon-intensity mapping for hydrogen-driven energy and economy. Cell Rep Phys Sci 2024;5(9). http://dx.doi.org/10.1016/j.xcrp.2024.102146.

[11] Gunawan TA, Williamson I, Raine D, Monaghan RFD. Decarbonising city bus networks in Ireland with renewable hydrogen. Int J Hydrog Energy 2021;46(57):28870–86. http://dx.doi.org/10.1016/j.ijhydene.2019.06.163.

[12] Arsie I, Battistoni M, Brancaleoni PP, Cipollone R, Corti E, Di Battista D, et al. A new generation of hydrogen-fueled hybrid propulsion systems for the urban mobility of the future. Energies 2023;17(1):34. http://dx.doi.org/10.3390/en17010034.

[13] Sharma S, Ghoshal SK. Hydrogen the future transportation fuel: From production to applications. Renew Sustain Energy Rev 2015;43:1151–8. http://dx.doi.org/10.1016/j.rser.2014.11.093.

[14] Nguyen T, Abdin Z, Holm T, Mérida W. Grid-connected hydrogen production via large-scale water electrolysis. Energy Convers Manage 2019;200:112108. http://dx.doi.org/10.1016/j.enconman.2019.112108.

[15] Sinigaglia T, Lewiski F, Martins MES, Siluk JCM. Production, storage, fuel stations of hydrogen and its utilization in automotive applications—A review. Int J Hydrog Energy 2017;42(39):24597–611. http://dx.doi.org/10.1016/j.ijhydene.2017.08.063.

[16] Ajanovic A, Glatt A, Haas R. Prospects and impediments for hydrogen fuel cell buses. Energy 2021;235:121340. http://dx.doi.org/10.1016/j.energy.2021.121340.

[17] Bethoux O. Hydrogen fuel cell road vehicles: State of the art and perspectives. Energies 2020;13(21):5843. http://dx.doi.org/10.3390/en13215843.

[18] Onorati A, Payri R, Vaglieco BM, Agarwal AK, Bae C, Bruneaux G, et al. The role of hydrogen for future internal combustion engines. Int J Engine Res 2022;23(4):529–40. http://dx.doi.org/10.1177/146808742210819.

[19] Stepień Z. A comprehensive overview of hydrogen-fueled internal combustion engines: Achievements and future challenges. Energies 2021;14(20):6504. http://dx.doi.org/10.3390/en14206504.

[20] Verhelst S. Recent progress in the use of hydrogen as a fuel for internal combustion engines. Int J Hydrog Energy 2014;39(2):1071–85. http://dx.doi.org/10.1016/j.ijhydene.2013.10.102.

[21] Desantes JM, Molina S, Novella R, Lopez-Juarez M. Comparative global warming impact and NOX emissions of conventional and hydrogen automotive propulsion systems. Energy Convers Manage 2020;221:113137. http://dx.doi.org/10.1016/j.enconman.2020.113137.

[22] Ricardo. Developing heavy-duty hydrogen powertrains for 2025+. 2023, https://mobex.io/webinars/developing-heavy-duty-hydrogen-powertrains-for-2025/. online documentation.

[23] Millo F, Rolando L, Fuso R, Zhao J. Development of a new hybrid bus for urban public transportation. Appl Energy 2015;157:583–94. http://dx.doi.org/10.1016/j.apenergy.2015.03.131.

[24] Halder P, Babaie M, Salek F, Shah K, Stevanovic S, Bodisco TA, et al. Performance, emissions and economic analyses of hydrogen fuel cell vehicles. Renew Sustain Energy Rev 2024;199:114543. http://dx.doi.org/10.1016/j.rser.2024.114543.

[25] Wu J, Yuan XZ, Martin JJ, Wang H, Zhang J, Shen J, et al. A review of PEM fuel cell durability: Degradation mechanisms and mitigation strategies. J Power Sources 2008;184(1):104–19. http://dx.doi.org/10.1016/j.jpowsour.2008.06.006.

[26] Zhang T, Wang P, Chen H, Pei P. A review of automotive proton exchange membrane fuel cell degradation under start-stop operating condition. Appl Energy 2018;223:249–62. http://dx.doi.org/10.1016/j.apenergy.2018.04.049.

[27] Sciarretta A, Guzzella L. Control of hybrid electric vehicles. IEEE Control Syst Mag 2007;27(2):60–70. http://dx.doi.org/10.1109/MCS.2007.338280.

[28] Li Q, Su T, Yin L, Xie S, Tan Y, Chen W, et al. Health management for PEMFC system long-term operation based on optimal temperature trajectory real-time optimization. IEEE Trans Ind Electron 2024;1–11. http://dx.doi.org/10.1109/TIE.2024.3436539.

[29] Li Q, Wang H, Wang T, Li X, Liu Y, Chen W, et al. Online diagnosis method of water management faults based on hybrid-frequency electrochemical impedance spectroscopy for PEMFC. IEEE Trans Transp Electrification 2024;1. http://dx.doi.org/10.1109/TTE.2024.3427401.

[30] Jahnke T, Futter G, Latz A, Malkow T, Papakonstantinou G, Tsotridis G, et al. Performance and degradation of proton exchange membrane fuel cells: State of the art in modeling from atomistic to system scale. J Power Sources 2016;304:207–33. http://dx.doi.org/10.1016/j.jpowsour.2015.11.041.

[31] Chen H, Pei P, Song M. Lifetime prediction and the economic lifetime of proton exchange membrane fuel cells. Appl Energy 2015;142:154–63. http://dx.doi.org/10.1016/j.apenergy.2014.12.062.

[32] Pei P, Chang Q, Tang T. A quick evaluating method for automotive fuel cell lifetime. Int J Hydrog Energy 2008;33(14):3829–36. http://dx.doi.org/10.1016/j.ijhydene.2008.04.048.

[33] Gao D, Jin Z, Zhang J, Li J, Ouyang M. Development and performance analysis of a hybrid fuel cell/battery bus with an axle integrated electric motor drive system. Int J Hydrog Energy 2016;41(2):1161–9. http://dx.doi.org/10.1016/j.ijhydene.2015.10.046.

[34] Yang D, Wang L, Yu K, Liang J. A reinforcement learning-based energy management strategy for fuel cell hybrid vehicle considering real-time velocity prediction. Energy Convers Manage 2022;274:116453. http://dx.doi.org/10.1016/j.enconman.2022.116453.

[35] Tang X, Zhou H, Wang F, Wang W, Lin X. Longevity-conscious energy management strategy of fuel cell hybrid electric vehicle based on deep reinforcement learning. Energy 2022;238:121593. http://dx.doi.org/10.1016/j.energy.2021.121593.

[36] Luca R, Whiteley M, Neville T, Shearing PR, Brett DJL. Comparative study of energy management systems for a hybrid fuel cell electric vehicle-a novel mutative fuzzy logic controller to prolong fuel cell lifetime. Int J Hydrog Energy 2022;47(57):24042–58. http://dx.doi.org/10.1016/j.ijhydene.2022.05.192.

[37] Wang Y, Moura SJ, Advani SG, Prasad AK. Power management system for a fuel cell/battery hybrid vehicle incorporating fuel cell and battery degradation. Int J Hydrog Energy 2019;44(16):8479–92. http://dx.doi.org/10.1016/j.ijhydene.2019.02.003.

[38] Desantes JM, Novella R, Pla B, Lopez-Juarez M. A modeling framework for predicting the effect of the operating conditions and component sizing on fuel cell degradation and performance for automotive applications. Appl Energy 2022;317:119137. http://dx.doi.org/10.1016/j.apenergy.2022.119137.

[39] Piras M, De Bellis V, Malfi E, Novella R, Lopez-Juarez M. Hydrogen consumption and durability assessment of fuel cell vehicles in realistic driving. Appl Energy 2024;358:122559. http://dx.doi.org/10.1016/j.apenergy.2023.122559.

[40] Sterlepper S, Fischer M, Claßen J, Huth V, Pischinger S. Concepts for hydrogen internal combustion engines and their implications on the exhaust gas aftertreatment system. Energies 2021;14(23):8166. http://dx.doi.org/10.3390/en14238166.

[41] Kuyumcu AM, Bingül B, Akar F, Yıldız A. Well-to-wheel carbon footprint and cost analysis of gasoline, diesel, hydrogen ICE, hybrid and fully electric city buses. Energy 2024;301:131685. http://dx.doi.org/10.1016/j.energy.2024.131685.

[42] Mousavi SB, Ahmadi P, Raeesi M. Performance evaluation of a hybrid hydrogen fuel cell/battery bus with fuel cell degradation and battery aging. Renew Energy 2024;227:120456. http://dx.doi.org/10.1016/j.renene.2024.120456.

[43] Singh M, Singla MK, Beryozkina S, Gupta J, Safaraliev M. Hydrogen vehicles and hydrogen as a fuel for vehicles: A-state-of-the-art review. Int J Hydrog Energy 2024;64:1001–10. http://dx.doi.org/10.1016/j.ijhydene.2024.03.325.

[44] Gürbüz H, Akçay H, Demirtürk S, Topalcı Ü. Techno-enviro-economic comparison analysis of a PEMFC and a hydrogen-fueled SI engine. Appl Therm Eng 2024;243:122528. http://dx.doi.org/10.1016/j.applthermaleng.2024.122528.

[45] Durkin K, Khanafer A, Liseau P, Stjernström-Eriksson A, Svahn A, Tobiasson L, et al. Hydrogen-powered vehicles: Comparing the powertrain efficiency and sustainability of fuel cell versus internal combustion engine cars. Energies 2024;17(5):1085. http://dx.doi.org/10.3390/en17051085.

[46] Depcik C, Cassady T, Collicott B, Burugupally SP, Li X, Alam SS, et al. Comparison of lithium ion batteries, hydrogen fueled combustion engines, and a hydrogen fuel cell in powering a small unmanned aerial vehicle. Energy Convers Manage 2020;207:112514. http://dx.doi.org/10.1016/j.enconman.2020.112514.

[47] Sari RL, Robles AF, Serrano JM, Cleary D. Techno-economic assessment of hydrogen as a fuel for internal combustion engines and proton exchange membrane fuel cells on long haul applications. Energy Convers Manage 2024;311:118522. http://dx.doi.org/10.1016/j.enconman.2024.118522.

[48] Rout C, Li H, Dupont V, Wadud Z. A comparative total cost of ownership analysis of heavy duty on-road and off-road vehicles powered by hydrogen, electricity, and diesel. Heliyon 2022;8(12). http://dx.doi.org/10.1016/j.heliyon.2022.e12417.

[49] Correa G, Muñoz PM, Rodriguez CR. A comparative energy and environmental analysis of a diesel, hybrid, hydrogen and electric urban bus. Energy 2019;187:115906. http://dx.doi.org/10.1016/j.energy.2019.115906.

[50] Coleman D, Kopp M, Wagner T, Scheppat B. The value chain of green hydrogen for fuel cell buses—A case study for the Rhine-main area in Germany. Int J Hydrog Energy 2020;45(8):5122–33. http://dx.doi.org/10.1016/j.ijhydene.2019.06.163.

[51] Golisano R, Scalabrini S, Arpaia A, Pesce F, Vassallo A, Borgia L, et al. PUNCH hydrogen internal combustion engine & KERS: An appealing value-proposition for green power pack. In: Proceedings of the 42nd international vienna motor symposium, vienna, Austria. 2021, p. 29–30.

[52] Millo F, Piano A, Rolando L, Accurso F, Gullino F, Roggio S, et al. Synergetic application of zero-, one-, and three-dimensional computational fluid dynamics approaches for hydrogen-fuelled spark ignition engine simulation. SAE Int J Engines 2021;15(03-15-04-0030):561–80, https://www.jstor.org/stable/27206788.

[53] Millo F, Rolando L, Piano A, Peiretti Paradisi B, Vinogradov A. Hydrogen powertrains: A comparison between different solutions for an urban bus. In: 22. internationales stuttgarter symposium: Automobil-und motorentechnik. Springer; 2022, p. 259–71.

[54] Paganelli G, Guerra T-M, Delprat S, Santin J-J, Delhom M, Combes E. Simulation and assessment of power control strategies for a parallel hybrid car. Int J Automob Eng 2000;214:705–17. http://dx.doi.org/10.1243/0954407001527583.

[55] UITP. Global bus survey 2019. 2023, https://www.uitp.org/publications/global-bus-survey/. online documentation.

[56] Ding Y, Cano ZP, Yu A, Lu J, Chen Z. Automotive li–ion batteries: Current status and future perspectives. Electrochem Energy Rev 2019;2:1–28. http://dx.doi.org/10.1007/s41918-018-0022-z.

[57] Schmuch R, Wagner R, Hörpel G, Placke T, Winter M. Performance and cost of materials for lithium-based rechargeable automotive batteries. Nat Energy 2018;3(4):267–78. http://dx.doi.org/10.1038/s41560-018-0107-2.

[58] Systems A. Nanophosphate® high power LithiumIon cell ANR26650m1-b. 2023, https://www.batteryspace.com/prod-specs/6610.pdf. online documentation.

[59] Catenaro E, Onori S. Experimental data of lithium-ion batteries under galvanostatic discharge tests at different rates and temperatures of operation. Data Brief 2021;35:106894. http://dx.doi.org/10.1016/j.dib.2021.106894.

[60] Catenaro E, Rizzo DM, Onori S. Experimental analysis and analytical modeling of enhanced-ragone plot. Appl Energy 2021;291:116473. http://dx.doi.org/10.1016/j.apenergy.2021.116473.

[61] Millo F, Rolando L, Pulvirenti L, Di Pierro G. A methodology for the reverse engineering of the energy management strategy of a plug-in hybrid electric vehicle for virtual test rig development. SAE Int J Electrified Veh 2021;11:113–32. http://dx.doi.org/10.4271/14-11-01-0009.

[62] Bianchi D, Rolando L, Serrao L, Onori S, Rizzoni G, Al-Khayat N, et al. Layered control strategies for hybrid electric vehicles based on optimal control. Int J Electr Hybrid Veh 2011;3(2):191–217. http://dx.doi.org/10.1504/IJEHV.2011.042147.

[63] Samsung. Introduction of samsung sdi's 94ah cells. 2023, https://cdn.shopify.com/s/files/1/0480/6521/6669/files/BMW_Samsung_SDI_94Ah_Datasheet.pdf?v=1605781107. online documentation.

[64] ZeEUS. ZeeUS ebus report #2 an updated overview of electric buses in Europe. 2023, https://zeeus.eu/uploads/publications/documents/zeeus-ebus-report-2.pdf. online documentation.

[65] Harper G, Sommerville R, Kendrick E, Driscoll L, Slater P, Stolkin R, et al. Recycling lithium-ion batteries from electric vehicles. Nature 2019;575(7781):75–86. http://dx.doi.org/10.1038/s41586-019-1682-5.

[66] Kivekäs K, Lajunen A, Vepsäläinen J, Tammi K. City bus powertrain comparison: Driving cycle variation and passenger load sensitivity analysis. Energies 2018;11(7):1755. http://dx.doi.org/10.3390/en11071755.

[67] TransportforLondon. London exhaust emissions study: A summary of the drive cycle development, test programme and comparison of test data compared with type approval data. 2020, http://content.tfl.gov.uk/london-exhaust-emissions-study-drive-cycle-development.pdf. online documentation.

[68] Millo F, Rolando L, Andreata M. Numerical simulation for vehicle powertrain development. In: Awrejcewicz J, editor. Numerical analysis. Rijeka: IntechOpen; 2011, http://dx.doi.org/10.5772/24111.

[69] Millo F, Rolando L, Piano A, Vinogradov A, Peiretti Paradisi B, et al. Comparison between different hydrogen fuelled powertrains for urban busses. vol. 1, Société Des Ingenieurs de l'Automobile; 2022, p. 21–30, URL https://iris.polito.it/retrieve/handle/11583/2972331/607022.

[70] Zhang J, Lu X, Xue J, Li B. Regenerative braking system for series hybrid electric city bus. World Electr Veh J 2008;2(4):363–9. http://dx.doi.org/10.3390/wevj2040363.

[71] Barbir F. Preface and acknowledgments. In: Barbir F, editor. PEM fuel cells. Burlington: Academic Press; 2005, p. xiii–v. http://dx.doi.org/10.1016/B978-012078142-3/50001-X, URL https://www.sciencedirect.com/science/article/pii/B978012078142350001X.

[72] Springer TE, Zawodzinski TA, Gottesfeld S. Polymer electrolyte fuel cell model. J Electrochem Soc 1991;138(8):2334–42. http://dx.doi.org/10.1149/1.2085971.

[73] Bellman R. Dynamic programming. Dover Publications; 1957, URL https://www.bibsonomy.org/bibtex/29cdd821222218ded252c8ba5cd712666/pcbouman.

[74] Onori S, Serrao L, Rizzoni G. Adaptive equivalent consumption minimization strategy for hybrid electric vehicles. In: Dynamic systems and control conference, vol. 44175, 2010, p. 499–505.

[75] Pulvirenti L, Rolando L, Millo F. Energy management system optimization based on an LSTM deep learning model using vehicle speed prediction. Transp Eng 2023;11:100160. http://dx.doi.org/10.1016/j.treng.2023.100160.

[76] Basma H, Mansour C, Haddad M, Nemer M, Stabat P. Comprehensive energy modeling methodology for battery electric buses. Energy 2020;207:118241. http://dx.doi.org/10.1016/j.energy.2020.118241.

[77] Zacharof N, Özener O, Broekaert S, Özkan M, Samaras Z, Fontaras G. The impact of bus passenger occupancy, heating ventilation and air conditioning systems on energy consumption and CO2 emissions. Energy 2023;272:127155. http://dx.doi.org/10.1016/j.energy.2023.127155.

[78] Department of Energy. DOE technical targets for polymer electrolyte membrane fuel cell component," accessed March 2024. 2024, https://www.energy.gov/eere/fuelcells/doe-technical-targets-polymer-electrolyte-membrane-fuel-cell-components. online documentation.

[79] Ahmadi P, Torabi SH, Afsaneh H, Sadegheih Y, Ganjehsarabi H, Ashjaee M. The effects of driving patterns and PEM fuel cell degradation on the lifecycle assessment of hydrogen fuel cell vehicles. Int J Hydrog Energy 2020;45(5):3595–608. http://dx.doi.org/10.1016/j.ijhydene.2019.01.165.

[80] Mansour S, Raeesi M. Performance assessment of fuel cell and electric vehicles taking into account the fuel cell degradation, battery lifetime, and heating, ventilation, and air conditioning system. Int J Hydrog Energy 2024;52:834–55. http://dx.doi.org/10.1016/j.ijhydene.2023.05.315.

[81] Burton T, Powers S, Burns C, Conway G, Leach F, Senecal K. A data-driven greenhouse gas emission rate analysis for vehicle comparisons. SAE Int J Electrified Veh 2023;12(1). http://dx.doi.org/10.4271/14-12-01-0006.